

# A study of the fine-structure constant dependence of radiative capture in Halo-EFT

Ulf-G. Meißner,<sup>1,2,3,\*</sup> Bernard Ch. Metsch,<sup>3,1,†</sup> and Helen Meyer<sup>1,2,‡</sup>

<sup>1</sup>*Helmholtz-Institut für Strahlen- und Kernphysik,*

*Rheinische Friedrich-Wilhelms Universität Bonn, D-53115 Bonn, Germany*

<sup>2</sup>*Bethe Center for Theoretical Physics, Rheinische Friedrich-Wilhelms Universität Bonn, D-53115 Bonn, Germany*

<sup>3</sup>*Institute for Advanced Simulation (IAS-4), Forschungszentrum Jülich, D-52425 Jülich, Germany*

(Dated: May 22, 2024)

We study the fine-structure constant dependence of the rates of some selected radiative capture reactions within the framework of so-called Halo Effective Field Theory in order to assess the adequacy of some assumptions made on the Coulomb penetrability. We find that this dependence deviates from that implied by a parameterization of the cross sections of this effect via a simple penetration factor. Some features of this fine-structure dependence are discussed, in particular its potential impact on the abundances of the light elements in primordial nucleosynthesis.

## I. INTRODUCTION

In Ref. [1] we made a re-assessment of the electromagnetic fine-structure constant dependence of the light element abundances in primordial nucleosynthesis or Big Bang nucleosynthesis (BBN). This required a description of the fine-structure constant dependence of the pertinent cross sections of the leading reactions in the BBN network. Only for the leading nuclear reaction, *i.e.* the radiative capture reaction  $p + n \rightarrow d + \gamma$  a detailed and sufficiently accurate theoretical description within the framework of pionless Effective Field Theory (EFT) is available, see [3]. For the other reactions we relied on a parameterization of the fine-structure constant dependence that accounted for the dependence of  $Q$ -values of the nuclear reactions through changes in the nuclear binding energies due to the Coulomb interaction of the protons as well as a modeling of the Coulomb penetration factors in the form

$$P(x) = \frac{x}{e^x - 1} \quad (1)$$

with

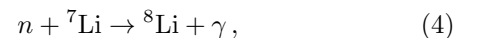
$$x = 2\pi \frac{Z_a Z_b \mu_{ab} c^2 \alpha}{c p} = \sqrt{\frac{E_G(\alpha)}{E}} \quad (2)$$

in terms of the so-called Gamow energy for a two-particle reaction channel  $ij$

$$E_G(\alpha) = 2\pi^2 Z_i^2 Z_j^2 \mu_{ij} c^2 \alpha^2 \quad (3)$$

and the center-of-mass (CMS) energy  $E$  or  $E + Q$  for the entrance and the exit channel, respectively. Here,  $p$  is the corresponding CMS momentum,  $Z_i$  the charge (in units of the elementary charge  $e$ ) of nuclide  $i$ ,  $\mu_{ij}$  the reduced mass,  $c$  is the speed of light and  $\alpha$  denotes the fine-structure constant. In addition we accounted for a

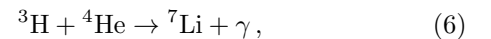
simple linear dependence on  $\alpha$  in case of radiative capture reactions as well as a trivial  $\alpha$  dependence reflecting the final momentum dependence if assuming dominance of dipole radiation, see [1]. We also noted in [1] that for some other radiative capture reactions an effective field theory description, *viz.* “Halo-EFT”, is available that potentially offers the possibility to study the  $\alpha$  dependence of the cross sections analytically and thus assess the validity of the assumptions made in [1]. For a comprehensive overview on applications of Halo-EFT to nuclear structure and reactions we refer to the review [2]. The purpose of the present paper is to study the  $\alpha$  dependence of the cross sections and the corresponding rates for the following radiative capture reactions: The neutron induced reaction



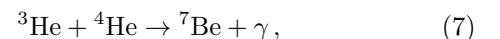
as treated in Refs. [4, 5], the proton induced reaction



as treated in Ref. [6] and the two reactions that are most relevant to BBN:



and



as treated in Refs. [7, 8]. Although in the present contribution we shall rely on the implementation as elaborated in Refs. [4]-[8] we like to mention that the  $n + {}^7\text{Li} \rightarrow {}^8\text{Li} + \gamma$  reaction was also treated within the Halo-EFT framework in Ref. [9]. Furthermore, earlier Halo-EFT work on the  $p + {}^7\text{Be} \rightarrow {}^8\text{B} + \gamma$  reaction can be found in Refs. [10, 11]. For a discussion on the  ${}^3\text{He} + {}^4\text{He} \rightarrow {}^7\text{Be} + \gamma$  reaction, we refer to [12].

The paper is organized as follows: In Sect. II we recapitulate the formulas for the radiative capture cross section in Halo-EFT. We then compare the results for the nominal  $\alpha$  value with experimental data in Sect. III. The results on the  $\alpha$  dependence of the cross sections

\* meissner@hiskp.uni-bonn.de

† metsch@hiskp.uni-bonn.de

‡ hmeyer@hiskp.uni-bonn.de

or astrophysical  $S$ -factors and the corresponding rates are discussed in Sect. IV. The impact on the changes of the light element abundances with a variation of the fine-structure constant is presented in Sect. V. We summarize our findings in Sect. VI. Some technicalities not given in Refs. [6]-[8] are relegated to the Appendices.

## II. BASIC FORMALISM

In Halo-EFT the nuclear system is assumed to consist of a “core”-system with mass  $m_c$ , charge number  $Z_c$  and spin  $s_c$  and a “valence”-system with mass  $m_v$ , charge number  $Z_v$  and spin  $s_v$ . Furthermore,  $M = m_c + m_v$  and  $\mu = m_c m_v / M$  denote the total mass and the reduced mass of the system, respectively. With  $L_i$  denoting the orbital angular momentum of the relative motion in the initial state the total spin and angular momentum in the initial state is given by  $\vec{S}_i = \vec{s}_c + \vec{s}_v$  and  $\vec{J}_i = \vec{S}_i + \vec{L}_i$ , respectively. Within the effective range expansion the initial state interaction is then specified by the parameters  $a_{\zeta_i}$ ,  $r_{\zeta_i}$ , and  $s_{\zeta_i}$ , ( $\zeta_i = S_i L_i J_i$ ) which for  $L_i = 0$  correspond to the  $s$ -wave scattering length, effective range and the first shape parameter, respectively.

The final state in the radiative capture reaction has mass  $M_f$ , charge number  $Z_f$ , excitation energy  $E_x$  and total nuclear spin  $J_f$ . In terms of partial waves  $^{S_f}L_f J_f$  the final state is written as

$$\begin{aligned} |M_f, E_x; J_f\rangle &= \sum_{s_f, L_f} a_{S_f, L_f} \left| \left[ [s_c \times s_v]^{S_f} \times L_f \right]^{J_f} \right\rangle \\ &= \sum_{\zeta} a_{\zeta_f} |\zeta_f\rangle \end{aligned} \quad (8)$$

with  $S_f$  the total spin of the di-nuclear-cluster and  $L_f$  the relative orbital angular momentum quantum number. The coefficients  $a_{S_f, L_f}$  are the amplitudes for the decomposition of the final state in terms of di-nuclear states. Then

$$B_{\zeta} = M - (M_f^{\zeta} + E_x^{\zeta})$$

is called the separation energy with respect to the clusters “ $v$ ” and “ $c$ ” and

$$\gamma_{\zeta} = \sqrt{2 M B_{\zeta}}$$

the binding momentum of this state. We define

$$k_C = Z_c Z_v \alpha \mu \quad (9)$$

as the inverse Bohr radius of a di-nuclear system in the case of charged particles.

### A. Electric dipole radiative capture

The formulas in this section are adopted from Ref. [8]. Assuming that the radiative capture proceeds through

an electric dipole transition and that only a single state contributes, the cross section is given by the expression

$$\begin{aligned} \sigma_{E1}(p) &= \frac{1}{16\pi M^2} \frac{1}{(2s_c + 1)(2s_v + 1)} \\ &\times \sum_{\zeta} |a_{\zeta}|^2 \frac{k_{\gamma}^{(\zeta)}}{p} \left| M_{E1}^{(\zeta)} \right|^2, \end{aligned} \quad (10)$$

where  $p$  is the magnitude of the relative momentum in the CMS with  $E = p^2 / (2\mu)$  the non-relativistic expression for the energy of the relative motion and

$$k_{\gamma}^{(\zeta)} = \frac{p^2 + \gamma_{\zeta}^2}{2\mu} \quad (11)$$

the non-relativistic approximation to the momentum of the photon in the final state.

The dimensionless amplitude squared reads

$$\begin{aligned} \left| M_{E1}^{(\zeta)} \right|^2 &= 64\pi \alpha (2J_f^{\zeta} + 1) \frac{(Z_v m_c - Z_c m_v)^2}{\mu \gamma_{\zeta}} \mathcal{N}(\eta_{\zeta}^{\zeta}, \rho_{\zeta}^{\zeta}) \\ &\times \left[ |\mathcal{A}(p)|^2 + 2 |Y(p)|^2 \right]. \end{aligned} \quad (12)$$

Here, we defined  $\eta_{\zeta}^{\zeta} = k_C / \gamma_{\zeta}$  and  $\rho_{\zeta}^{\zeta} = \rho_1^{\zeta} / \gamma_{\zeta}$  with  $\rho_1^{\zeta} = \hbar c / r_1^{\zeta}$  the effective momentum and  $r_1^{\zeta}$  the effective range in the channel  $\zeta$ . The normalisation is given by

$$\begin{aligned} \mathcal{N}(\eta, \rho) &= \frac{2\pi}{-\rho + 4\eta h(\eta) + 2\eta^2 (\eta^2 - 1) h'(\eta)}, \end{aligned} \quad (13)$$

where

$$h(\eta) = \psi(\eta) + \frac{1}{2\eta} - \log(\eta) \quad (14)$$

and  $\psi(\eta) = \Gamma'(\eta) / \Gamma(\eta)$  is the digamma function. The normalisation is thus completely determined by the binding energy of the di-nuclear cluster (via  $\eta$ ) and the effective momentum (via  $\rho$ ) in the final state. In case of a neutral cluster  $k_C = 0$  and thus  $\eta = k_C / \gamma = 0$ . Then

$$\mathcal{N}(\eta, \rho)|_{\eta=0} = -\frac{2\pi \gamma}{\rho + 3\gamma}. \quad (15)$$

With  $\eta_p = k_C / p$  the capture from the initial  $s$ -wave is given by the amplitude

$$\left| \frac{\mathcal{A}(p)}{C_0(\eta_p)} \right| = \left| X(p) - \frac{2\pi}{\mu^2} \frac{B(p) + \mu J_0(p) + \mu^2 k_{\gamma}^{(\zeta)} L_{E1}^{(\zeta)}}{[C_0(\eta_p)]^2 p (\cotan(\delta_0) - i)} \right|, \quad (16)$$

where  $L_{E1}^{(\zeta)}$  is the low-energy constant of the the two-body current contact term and

$$\begin{aligned} X(p) &= 1 + \frac{2}{3} \kappa \frac{\Gamma(2 + \eta_{\gamma})}{C_0(\eta_p)} \int_0^{\infty} d\rho W_{-\eta_{\gamma}, \frac{3}{2}}(2\kappa\rho) \\ &\times \left[ -\frac{F_0(\eta_p, \rho)}{\rho} + \partial_{\rho} F_0(\eta_p, \rho) \right], \end{aligned} \quad (17)$$

is the  $s$ -wave contribution without initial state strong interactions in terms of Coulomb functions  $F_\ell$  and Whittaker functions  $W_{\eta,\mu}$ , which are the solutions to the pure Coulomb problem. In the case where  $k_C = 0$  (*i.e.* if a neutral particle is involved) this reduces to

$$X(p)|_{\eta_\gamma=0} = 1 - \frac{2}{3} \frac{p^2}{p^2 + \gamma^2}. \quad (18)$$

The  $s$ -wave contribution from strong initial-state interactions is given by

$$\begin{aligned} \frac{B(p) + \mu J_0(p)}{\mu^2 p} &= \frac{1}{3\pi} \frac{i - \kappa^3}{1 + \kappa^2} + \eta_p \frac{C(p)}{\mu^2} + \frac{\Delta B(p)}{\mu^2 p} \\ &\quad - \frac{\eta_p}{2\pi} \left[ 2h(i\eta_p) + 2\gamma_E - \frac{5}{3} + \log(4\pi) \right]. \end{aligned} \quad (19)$$

Here, the function  $C(p)$  is given by a double integral, treated in App. A and the finite contribution  $\Delta B(p)$  is evaluated as follows: The integrand

$$\begin{aligned} \mathcal{B}(\kappa, \eta_\gamma; \rho) &= -\frac{\kappa}{3\pi} \Gamma(2 + \eta_\gamma) \Gamma(1 + i\kappa\eta_\gamma) W_{-\eta_\gamma, \frac{3}{2}}(2\kappa\rho) \\ &\quad \times \left[ -\frac{1}{\rho} W_{-i\kappa\eta_\gamma, \frac{1}{2}}(-2i\rho) + \partial_\rho W_{-i\kappa\eta_\gamma, \frac{1}{2}}(-2i\rho) \right] \end{aligned} \quad (20)$$

where  $\kappa = \eta_p/\eta_\gamma = \gamma/p$ , in

$$\frac{B(p)}{\mu^2 p} = \int_0^\infty d\rho \mathcal{B}(\kappa, \eta_\gamma; \rho), \quad (21)$$

is quadratically divergent for  $\rho \rightarrow 0$ . Noting that the integrand depends on  $\alpha$  via  $\eta_\gamma = k_C/\gamma$  and  $k_C \propto \alpha$ , the integrand can be regularized by subtracting the terms from zero and single photon contributions, *i.e.* the terms of  $\mathcal{O}(\alpha^0)$  and  $\mathcal{O}(\alpha^1)$ . Then, with

$$\alpha \frac{\partial \mathcal{B}(\alpha)}{\partial \alpha} = \eta_\gamma \frac{\partial \mathcal{B}(\kappa, \eta_\gamma; \rho)}{\partial \eta_\gamma},$$

the finite contribution<sup>1</sup> is given by

$$\begin{aligned} \frac{\Delta B(p)}{\mu^2 p} &= \int_0^\infty d\rho \left[ \mathcal{B}(\kappa, \eta_\gamma; \rho) \right. \\ &\quad \left. - \mathcal{B}(\kappa, 0; \rho) - (\partial_{\eta_\gamma} \mathcal{B})(\kappa, 0; \rho) \cdot \eta_\gamma \right] \end{aligned} \quad (22)$$

which can be integrated numerically<sup>2</sup>. For neutral parti-

<sup>1</sup> As pointed out in Ref. [8] the divergent pieces of  $B$  cancel the divergent pieces in  $J_0$ , this was accounted for in arriving at Eq. (19).

<sup>2</sup> The partial derivative involved might be difficult to find analytically. Although in principle not particularly stable, one could use numerical approximations to the (partial) derivative of a function  $\mathcal{B}(\kappa, \eta_\gamma; \rho)$ , such as (with  $\mathcal{B}_j = \mathcal{B}(\kappa, j h; \rho)$ ):

$$\begin{aligned} (\partial_{\eta_\gamma} \mathcal{B}(\kappa, \eta_\gamma, \rho))|_{\eta_\gamma=0} &= \frac{8(\mathcal{B}_{+1} - \mathcal{B}_{-1}) - (\mathcal{B}_{+2} - \mathcal{B}_{-2})}{12h} + \mathcal{O}(h^4) \\ &= \frac{45(\mathcal{B}_{+1} - \mathcal{B}_{-1}) - 9(\mathcal{B}_{+2} - \mathcal{B}_{-2}) + (\mathcal{B}_{+3} - \mathcal{B}_{-3})}{60h} + \mathcal{O}(h^6) \end{aligned}$$

for some small finite  $h$ .

cles, *i.e.*  $k_C = 0$ , one obtains

$$\left. \frac{B(p) + \mu J_0(p)}{\mu^2 p} \right|_{k_C=0} = \frac{1}{3\pi} \frac{i - \kappa^3}{1 + \kappa^2} - \frac{i}{2\pi}. \quad (23)$$

Finally, the contribution from the initial  $d$ -wave states to the capture process is given by the amplitude

$$\begin{aligned} Y(p) &= \frac{2}{3} \kappa \Gamma(2 + \eta_\gamma) \int_0^\infty d\rho W_{-\eta_\gamma, \frac{3}{2}}(2\kappa\rho) \\ &\quad \times \left[ \frac{2F_2(\eta_p, \rho)}{\rho} + \partial_\rho F_2(\eta_p, \rho) \right] \end{aligned} \quad (24)$$

which for  $k_C = 0$  reduces to

$$Y(p)|_{k_C=0} = \frac{2}{3} \frac{p^2}{p^2 + \gamma^2}. \quad (25)$$

## B. Magnetic dipole radiative capture

In case of single nucleon radiative capture there are additional relevant contributions from magnetic dipole transitions to the final states.

### 1. Neutron induced magnetic dipole contribution

In case of the  $n + {}^7\text{Li} \rightarrow {}^8\text{Li} + \gamma$  reaction we recapitulate the formulas from Ref. [5]. Earlier work on this reaction, including the  $M1$ -contribution, can be found in Ref. [4].

The cross section for the  $M1$  contribution to the radiative capture in the  ${}^7\text{Li} + n \rightarrow {}^8\text{Li} + \gamma$  reaction through the  $3^+$  resonance according to Ref. [4] is given by

$$\begin{aligned} \sigma_{M1}(p) &= \frac{1}{14} \frac{7}{3} \frac{\alpha \mu}{m_p^2} \left| h^2 \mathcal{Z}^{(\zeta)} \right| \left( \frac{k}{p} \right)^3 \\ &\quad \times \left| \frac{p^2}{-\frac{1}{a_1^{(3)} + \frac{1}{2} r_1^{(3)} p^2} - i p^3} \right|^2 \left\{ \left| \frac{2}{3} \frac{\gamma^3 - i p^3}{\gamma^2 + p^2} K^{(2)} + \beta^{(2)} \right|^2 \right. \\ &\quad \left. + \left| \frac{2}{3} \frac{\gamma^3 - i p^3}{\gamma^2 + p^2} K^{(1)} + \beta^{(1)} \right|^2 \right\}, \end{aligned} \quad (26)$$

with  $m_p$  the proton mass. The asymptotic normalization of the final  ${}^8\text{Li}$ -states ( $\zeta = 2^+$  for the ground state or  $\zeta = 1^+$  for the first excited state) with binding momentum  $\gamma^{(\zeta)}$  is given by

$$h^2 \mathcal{Z}^{(\zeta)} = -\frac{2\pi}{3\gamma^{(\zeta)} + r_1^{(\zeta)}},$$

the gyro-magnetic factors in the  ${}^5P_3 \rightarrow {}^3P_2$  and the

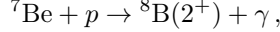
${}^5P_3 \rightarrow {}^5P_2$   $M1$ -transitions are given by

$$\begin{aligned} K^{(1)} &= \sqrt{\frac{3}{2}} \left( \frac{3}{2} g_c - \frac{3}{2} g_v \right), \\ K^{(2)} &= \sqrt{\frac{3}{2}} \left( \frac{3}{2} g_c - \frac{3}{2} g_v \right), \\ K^{(2)} &= \sqrt{\frac{3}{2}} \left( \frac{3}{2} g_c + \frac{1}{2} g_v + 2 \mu m_n \frac{Z_c}{m_c^2} \right), \end{aligned} \quad (27)$$

in terms of the gyro-magnetic ratios  $g_c$  and  $g_v$  describing the magnetic moments of the core and the valence system, respectively, and  $\beta^{(i)}$ ,  $i = 1, 2$  are constants reflecting the two-body current terms. Finally,  $a_1^{(3)}$  and  $r_1^{(3)}$  are the scattering volume and the effective momentum in the  ${}^5P_3$  scattering channel.

## 2. Proton induced magnetic dipole contribution

This section summarizes the results quoted in Ref. [6] for the  $M1$  contribution in the reaction



through the  $1^+$  resonance. Considered is only the  ${}^5P_1 \rightarrow {}^5P_2$  transition assuming that the  $1^+$  resonance is dominantly a proton  $p_{\frac{1}{2}}$  coupled to the  ${}^7\text{Be}(\frac{3}{2}^-)$  ground state with the amplitude

$$\left\langle \left[ \frac{3^-}{2} \times \left[ \frac{1^+}{2} \times 1^- \right]^{\frac{1}{2}} \right]^1 \middle| \left[ \left[ \frac{3^-}{2} \times \frac{1^+}{2} \right]^2 \times 1^- \right]^1 \right\rangle = \sqrt{\frac{5}{6}}. \quad (28)$$

The cross section for a magnetic dipole radiative reaction through the  $1^+$  resonance is then given by [6]

$$\sigma_{M1}(p) = \frac{1}{16\pi M^2} \frac{1}{6} \sum_{\zeta} \frac{(k_{\gamma}^{(\zeta)})^3}{p^3} |M_{M1}^{(\zeta)}|^2. \quad (29)$$

The squared matrix element reads

$$\begin{aligned} |M_{M1}^{(\zeta)}|^2 &= (2J_f^{(\zeta)} + 1) \mu^3 \frac{8\pi M^2 \alpha}{m_p^2} \frac{|\mathcal{A}_1(p)|^2}{|C_1(\eta_p)|^2} \\ &\quad \times \frac{2\pi}{\mu} \mathcal{Z}^{(5P_2)} \frac{\mu^2}{432 \pi^4} |\bar{L}_{22}(p)|^2, \end{aligned} \quad (30)$$

where

$$\begin{aligned} \bar{L}_{22}(p) &= \frac{2\pi}{\mu} \left\{ \frac{9\pi}{\sqrt{40}} \left[ 3g_c + g_v + 4\mu m_p \left( \frac{Z_{\phi}}{m_{\phi}^2} + \frac{Z_{\psi}}{m_{\psi}^2} \right) \right] \right. \\ &\quad \left. \times \frac{\bar{D}(p, \gamma_{\zeta})}{\mu^2} - \beta_{22} \right\} \end{aligned} \quad (31)$$

with  $\vec{\mu}_c = g_c \vec{J}_c$  and  $\mu_v = g_v \vec{J}_v$  the (spin) magnetic moments of the constituents  $c, v$  of the di-nuclear system and

$$\vec{\mu}_L = \mu m_p \left( \frac{Z_c}{m_c^2} + \frac{Z_v}{m_v^2} \right) \vec{L}$$

the magnetic moment due to the current associated with the relative orbital motion.<sup>3</sup>

Furthermore

$$\frac{\bar{D}(p)}{\mu^2 \gamma} = \frac{1}{3\pi} \frac{i\kappa^3 - 1}{1 + \kappa^2} + \eta_{\gamma} \frac{D'(\eta_p, \kappa)}{\mu^2} + \frac{\Delta D(k_C; p, \gamma)}{\mu^2 \gamma}, \quad (32)$$

where we defined  $\rho = pr$ ,  $\eta_{\gamma} = k_C/\gamma$ ,  $\kappa = \gamma/p$ ,  $\eta_p = \kappa \eta_{\gamma} = k_C/p$ . The integrand

$$\begin{aligned} \mathcal{D}(\kappa, \eta_{\gamma}; \rho) &= -i \frac{\kappa}{3\pi} \Gamma(2 + i\kappa \eta_{\gamma}) \Gamma(2 + \eta_{\gamma}) \\ &\quad \times W_{-\eta_{\gamma}, \frac{3}{2}}(2\kappa\rho) W_{-i\eta_p, \frac{3}{2}}(-2i\rho) \end{aligned} \quad (33)$$

in

$$D(k_C; p, \gamma) = \mu^2 p \int_0^{\infty} d\rho \mathcal{D}(\kappa, \eta_{\gamma}; \rho) \quad (34)$$

is again divergent for  $\rho \rightarrow 0$ . By subtracting the zero and single photon contributions one then defines the finite term

$$\begin{aligned} \Delta D(k_C; p, \gamma) &= \mu^2 p \int_0^{\infty} d\rho \left[ \mathcal{D}(\kappa, \eta_{\gamma}; \rho) \right. \\ &\quad \left. - \mathcal{D}(\kappa, 0; \rho) - (\partial_{\eta_{\gamma}} \mathcal{D})(\kappa, 0; \rho) \cdot \eta_{\gamma} \right]. \end{aligned} \quad (35)$$

The evaluation of the second term  $D'(\eta_p, \kappa)$  on the r.h.s. of Eq. (32) is given in App. B.

The initial-state interaction in the  ${}^5P_1$  channel is given by the amplitude

$$\begin{aligned} \gamma^2 \mathcal{A}_1(p) &= \frac{2\pi \gamma}{\mu} \\ &\quad \times \frac{9(C_1(\eta_p))^2 e^{i2\sigma_1}}{-\frac{1}{a_1^{(5P_1)} p^2 \gamma} + \frac{1}{2} \frac{r^{(5P_1)}}{\gamma} - 2 \frac{p}{\gamma} \eta_p (\eta_p^2 + 1) H(\eta_p)}, \end{aligned} \quad (36)$$

where  $a^{(5P_1)}$  is the scattering volume and  $r^{(5P_1)}$  the effective momentum to reproduce the  $1^+$  resonance with position  $E_R = p_R^2/(2\mu) = 0.630(3)$  MeV and width  $\Gamma_R = 0.0357(6)$  MeV. The normalization of the final state is determined by

$$\begin{aligned} \gamma \frac{2\pi}{\mu} \mathcal{Z}^{(5P_2)} &= \\ &= \frac{2\pi}{-\rho_{\gamma} + 2\eta_{\gamma}^2(\eta_{\gamma}^2 - 1) h'(\eta_{\gamma}) + 4\eta_{\gamma} h(\eta_{\gamma})} \end{aligned} \quad (37)$$

with  $\rho_{\gamma} = r_1^{(5P_2)}/\gamma$ .

<sup>3</sup> Note that the current due to the velocity of fragment  $i$  is given by the operator  $(Z_i e)/(m_i) \hat{p}_i$ . Accordingly the associated orbital magnetic moment, expressed in units of  $\mu_N = (e\hbar c)/(2m_p c^2)$ , reads  $\mu_i = Z_i (m_p/m_i) \mu_N \hat{L}_i$  with  $L_i$  the angular momentum of fragment  $i$ .

### III. CROSS SECTIONS, ASTROPHYSICAL S-FACTORS AND REACTION RATES.

The cross sections  $\sigma$  or the corresponding astrophysical  $S$ -factors given as

$$S(E) = E \sigma(E) e^{\sqrt{E_G/E}} \quad (38)$$

with  $E_G$  the Gamow energy in the entrance channel, were calculated according to the formulas given in the previous section, Sect. II. The nuclear structure parameters are given in Tab. I, while the reaction parameters for the nucleon induced reactions are given in Tab. II and for the radiative capture to  ${}^7\text{Li}$  and  ${}^7\text{Be}$  are given in Tab. III.

TABLE I. Nuclear structure data: Nuclear mass in MeV, spin/parity  $J^\pi$ , excitation energy  $E_x$  in MeV, binding momentum  $\gamma$  with respect to the di-nuclear system in MeV, the gyro-magnetic ratio  $g$  and the ground state nuclear Coulomb energy  $V_C$  in MeV [1].

Nucleus	Mass	$J^\pi$	$E_x$	$\gamma$	$g$	$V_C$
$p$	938.2721	$\frac{1}{2}^+$	0	-	5.5857	0
$n$	939.5654	$\frac{1}{2}^+$	0	-	-3.8261	0
${}^3\text{H}$		$\frac{1}{2}^+$	0	-	-	0
${}^3\text{He}$	2808.3916	$\frac{1}{2}^+$	0	-	-	0.6884
${}^4\text{He}$	3727.3794	$0^+$	0	-	-	0.7588
${}^7\text{Li}$	6533.8330	$\frac{3}{2}^-$	0	88.9099	2.1710	1.5994
		$\frac{1}{2}^-$	0.4776	79.8429	-	-
${}^7\text{Be}$	6534.1841	$\frac{3}{2}^-$	0	71.2970	-0.9329	2.7117
		$\frac{1}{2}^-$	0.4291	60.8999	-	-
${}^8\text{Li}$	7471.3658	$2^+$	0	57.7872	-	1.6491
		$1^+$	0.9808	41.5694	-	-
${}^8\text{B}$	7472.3201	$2^+$	0	14.9465	-	4.2119

The reaction rate in thermal equilibrium at temperature  $T$  then follows from the cross section via

$$\gamma(T) = N_A \sqrt{\frac{8}{\pi \mu (kT)^3}} \int_0^\infty dE \sigma(E) E e^{-\frac{E}{kT}}, \quad (39)$$

where  $N_A$  is the Avogadro number and  $k$  the Boltzmann constant. Essentially, this expression for the rate has the form of a Laplace-transform of the cross section multiplied by the CM-energy.

In the next subsections we present the resulting cross sections or astrophysical  $S$ -factors as well as the corresponding rates according to Eq. (39) for the four reactions studied here, all calculated at the present value of the fine-structure constant that we shall call the nominal value of  $\alpha$  given by

$$\alpha_0 = 7.2973525693(11)10^{-3} = 1/137.035999084(2) \quad (40)$$

from Ref. [13]. For each of the reactions considered here we present the calculated rates for two parameter sets used in the Halo-EFT calculations in order to give an impression of the systematic uncertainty. In addition we

TABLE II. Reaction parameters for the nucleon induced radiative capture reactions:  $s$ -wave scattering length  $a_0$  in fm,  $p$ -wave scattering volume  $a_1$  in  $\text{fm}^3$ ,  $p$ -wave effective momentum  $r_1$  in MeV, two-body current parameter  $\beta^{(1)} = \beta^{(2)} = \beta$  for the neutron induced reaction,  $\beta = \beta_{22}$  for the proton induced reaction, both in MeV.  $r_1({}^5P_2)^*$  is the value used in calculating the  $M1$  contribution. For the  ${}^7\text{Li}(n, \gamma){}^8\text{Li}$  reaction the parameter sets ‘‘A’’ and ‘‘ANC’’ correspond to those called ‘‘EFT A’’ and ‘‘EFT ANC’’ in Ref. [5], respectively. For the  ${}^7\text{Be}(p, \gamma){}^8\text{B}$  reaction the parameter sets ‘‘NNLO’’ and ‘‘ANC’’ correspond to those called ‘‘EFT<sub>gs</sub> I NNLO’’ and those related to a determination from A(symptotic) N(ormalization) C(oefficients), respectively, see Ref. [6].

Parameter	${}^7\text{Li}(n, \gamma){}^8\text{Li}$		${}^7\text{Be}(p, \gamma){}^8\text{B}$	
	A	ANC	NNLO	ANC
$a_0({}^3S_1)$	0.87	0.87	17.34	17.34
$a_0({}^5S_2)$	-3.63	-3.63	-3.18	-3.18
$r_1({}^3P_2)$	-290.0707	-605.6995	-173.0	-176.8
$r_1({}^5P_2)$	-290.0707	-270.0028	-32.92	-40.31
$r_1({}^5P_2)^*$	-290.1	-290.1	-30.00	-30.00
$r_1({}^3P_1)$	-473.5848	-638.1095		
$a_1({}^5P_1)$			-108.13	-108.13
$r_1({}^5P_1)$	-473.5848	-498.0909	-111.23	-111.23
$a_1({}^5P_3)$	-77.0136	-547.1		
$r_1({}^5P_3)$	-77.0136	-547.1		
$\beta$	170.0	170.0	375.0	375.0

TABLE III. Reaction parameters for the  ${}^3\text{H} + {}^4\text{He} \rightarrow {}^7\text{Li} + \gamma$  and  ${}^3\text{He} + {}^4\text{He} \rightarrow {}^7\text{Be} + \gamma$  reactions: The  $s$ -wave scattering length  $a_0$  in fm, the  $s$ -wave effective range  $r_0$  in fm, the  $s$ -wave shape parameter  $s_0$  in  $\text{fm}^3$ , the  $p$ -wave effective momentum  $r_1$  in MeV, the  $p$ -wave shape parameter  $s_1$  in fm and the LEC. The parameter sets labeled ‘‘fit’’, ‘‘A’’ and ‘‘fit’’, ‘‘AII’’ correspond to those labeled ‘‘ $\chi^2$ ’’, ‘‘Model A’’ and ‘‘ $\chi^2$ ’’ and ‘‘Model AII’’ in Ref. [8] for these two reactions, respectively.

Parameter	${}^4\text{He}({}^3\text{H}, \gamma){}^7\text{Li}$		${}^4\text{He}({}^3\text{He}, \gamma){}^7\text{Be}$	
	fit	A	fit	AII
$a_0({}^2S_{\frac{1}{2}})$	17.0	13.0	22.0	40.0
$r_0({}^2S_{\frac{1}{2}})$	0.6	-0.1	1.2	1.09
$s_0({}^2S_{\frac{1}{2}})$	2.0	11.0	-0.9	-2.2
$r_1({}^2P_{\frac{1}{2}})$	-129.0	-230.0	-41.9	-45.0
$r_1({}^2P_{\frac{3}{2}})$	-149.0	-190.0	-55.4	-59.0
$s_1({}^2P_{\frac{1}{2}})$	-	-	1.74	1.84
$s_1({}^2P_{\frac{3}{2}})$	-	-	1.59	1.69
LEC( ${}^2P_{\frac{1}{2}}$ )	1.5	4.0	0.83	1.07
LEC( ${}^2P_{\frac{3}{2}}$ )	1.44	2.2	0.78	1.02

compare the resulting rates with those used in the original versions of some publicly available BBN codes: *viz.* NUC123 [14], AlterBBN [15, 16], ParthENoPE [17–19] and PRIMAT [20], if available. These were also considered in our study [1] mentioned in the introduction. The most recent code PRyMordial, see [21, 22], by default uses the PRIMAT-rates and thus in this context is not discussed separately.

### A. The $n + {}^7\text{Li} \rightarrow {}^8\text{Li} + \gamma$ reaction

In this case  $Z_v = 0, Z_c = 3, s_v = 1/2, s_c = 3/2$  and  $Z_f = 4$  with  $J_f = 2$  for the ground state and  $J_f = 1$  for the excited state. The final  $2^+$  state is supposed to be an equal mixture of the  ${}^3P_2$  and  ${}^5P_2$  states, *i.e.*

$$|2^+\rangle = \frac{1}{\sqrt{2}} |{}^3P_2\rangle + \frac{1}{\sqrt{2}} |{}^5P_2\rangle, \quad (41)$$

while the excited  $1^+$  state is supposed to be

$$|1^+\rangle = -\frac{1}{\sqrt{6}} |{}^3P_1\rangle + \sqrt{\frac{5}{6}} |{}^5P_1\rangle. \quad (42)$$

The total radiative capture cross section in this case is given by the sum of the expression for the electric dipole contribution given in Eqs. (10,12) with the special formulas for  $k_C = 0$  given in Eqs. (15,18,23,25) and the magnetic dipole contribution of Eq. (26).

The resulting cross section (scaled with the laboratory neutron velocity) is compared to the experimental data in Fig. 1.

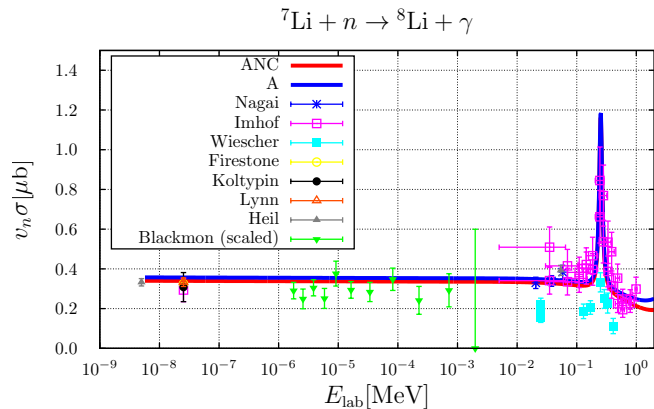


FIG. 1. Cross section (scaled with the laboratory neutron velocity  $v_n/c$ ) as a function of the laboratory neutron energy compared to experimental data: Nagai [23], Imhof [24], Wiescher [25], Firestone [26], Koltypin [27], Lynn [28], Heil [29], Blackmon [30]. The latter data were divided by the branching ratio 0.89 for the ground state in order to also account for the  $1^+$  final state contribution such that these data now represent the total capture cross section.

The calculated rates for the parameter sets “A” and “ANC” (these correspond to the parameter sets called “EFT A” and “EFT ANC” in Ref. [5], respectively; “ANC” standing for: “parameters corresponding to empirical A(symptotic) N(ormalization) C(oefficient)”) are compared to the rates as parameterized in NUC123 [14], PArthENoPE [17–19] and AlterBBN [15, 16] as well as to the rate resulting from the following novel parameterization of the cross section, accounting for the  $1^+$  resonance

via a non-relativistic Breit-Wigner parameterization

$$\sqrt{E} \sigma(E) = 0.0675 \frac{1 - 0.045 E + 0.7 E^2}{1 + 0.001 E + 0.7 E^2} + \frac{0.018}{1 + 5000.0 (E - 0.2215)^2},$$

(in  $\text{mb MeV}^{\frac{1}{2}}$ , with  $E$  in MeV) (43)

in Fig. 2. Indeed this parameterization yields a rate very similar to those of the Halo-EFT calculation.

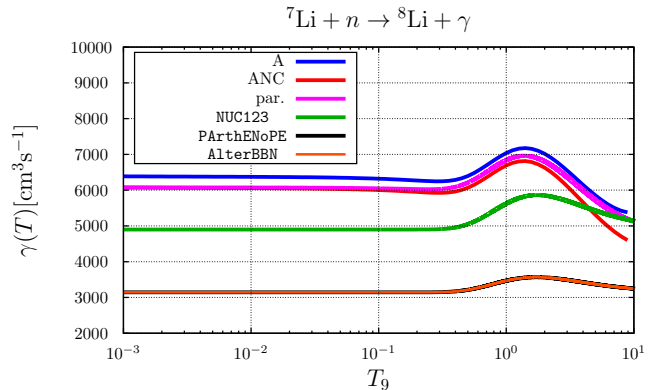


FIG. 2. Comparison of the temperature-dependent rate for the  $n + {}^7\text{Li} \rightarrow {}^8\text{Li} + \gamma$  reaction. Here,  $T_9 = T/10^9$  K. The blue and red curves represent the results from the parameter sets “A” and “ANC”, respectively, the purple curve is based on the parameterization of Eq. (43), the green curve is the rate used in NUC123 [14], the curves for the parameterizations in PArthENoPE [17–19] (black curve) and AlterBBN [15, 16] (brown curve) are identical.

### B. The $p + {}^7\text{Be} \rightarrow {}^8\text{B} + \gamma$ reaction

In this case  $Z_v = 1, Z_c = 4, s_v = 1/2, s_c = 3/2$  and  $Z_f = 5$  with  $J_f = 2$  for the ground state, which, as the corresponding ground state of the mirror nucleus is supposed to be an equal mixture of the  ${}^3P_2$  and  ${}^5P_2$  states. The total radiative capture cross section is given by the sum of the expression for the electric dipole contribution in Eqs. (10,12) with  $k_C \neq 0$  and the resonant magnetic dipole contribution as given in Eq. (29).

The resulting  $S$ -factor

$$S(E) = 0.018 \frac{1 + 0.3 E + 0.125 E^2}{1 + 0.017 E^2} + \frac{0.090}{1 + 2500.0 (E - 0.63)^2},$$

(in MeV mb, with  $E$  in MeV). (44)

is compared to experimental data and to the parameterization of Eq. (44) thereof in Fig. 3.

The calculated rate for the parameter sets “NNLO” and “ANC”, where these labels refer to the parameter sets labeled “EFT<sub>gs</sub> I NNLO” and those related

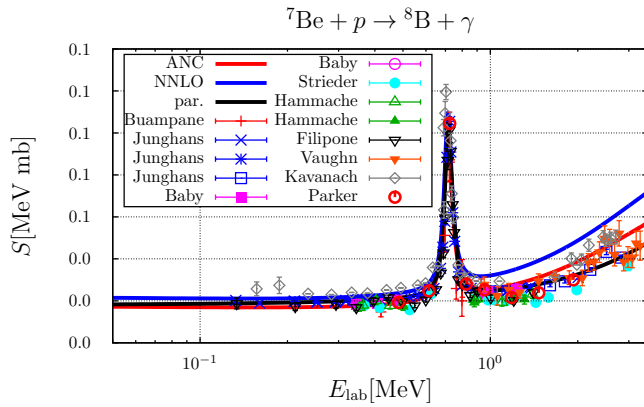


FIG. 3.  $S$ -factor as a function of the laboratory proton energy compared to experimental data: Buampane [31], Junghans [32–35], Baby [36–38], Strieder [39], Hammache [40], Filipone [41, 42], Vaughn [43], Kavanach [44], Parker [45]. The blue and red curve correspond to the parameter sets “NNLO” and “ANC”, respectively. The purple curve represents the parameterization given in Eq. (44).

to a determination from A(symptotic) N(ormalization) C(oefficients), respectively, see Ref. [6], are compared to the rates as parameterized in NUC123 [14], PArthENoPE [17–19] and AlterBBN [15, 16] as well as to the rate corresponding to the parameterization of the  $S$ -factor of Eq. (44) in Fig. 4.

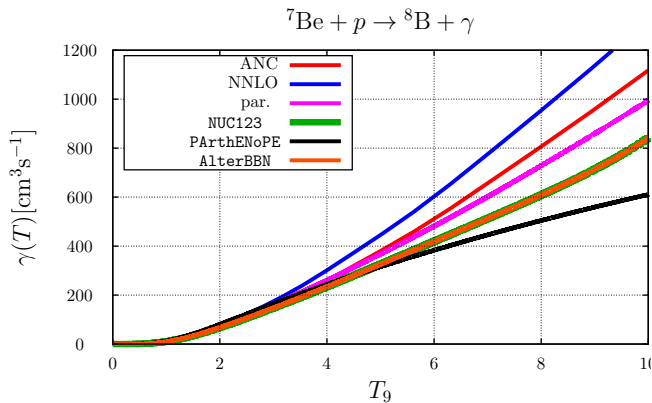


FIG. 4. Comparison of the temperature ( $T_9 = T/10^9$  K) dependent rate for the  $p + {}^7\text{Be} \rightarrow {}^8\text{B} + \gamma$  reaction. The blue and red curves represent the parameter sets “NNLO” and “ANC”, respectively, the purple curve is based on the parameterization of Eq. (44), the black curve is the rate used in PArthENoPE [17–19], the curves for the parameterizations in AlterBBN [15, 16] (brown curve) and NUC123 [14] (green curve) are identical.

### C. The ${}^3\text{H} + {}^4\text{He} \rightarrow {}^7\text{Li} + \gamma$ reaction

In this case  $Z_v = 1$ ,  $Z_c = 2$ ,  $s_v = 1/2$ ,  $s_c = 0$  and  $Z_f = 3$  with  $J_f = 3/2$  for the ground state and  $J_f = 1/2$  for the

first excited state. The radiative capture cross section is determined by electric dipole contributions only, *i.e.* by the expression for the electric dipole contribution in Eqs. (10,12) with  $k_C \neq 0$ . The parameter sets labeled “fit” and “A” correspond to the parameter sets labeled “ $\chi^2$ ” and “Model A” in Ref. [8], respectively.

The  $S$ -factor for this reaction

$$S(E) = 0.01 \frac{1 - 1.15E + 1.0E^2}{1 + 0.01E + 0.5E^2} \quad (\text{in MeV mb, with } E \text{ in MeV}). \quad (45)$$

is compared to experimental data and to the parameterization used in Ref. [1] as well as an improved parameterization, see Eq. (45), thereof in Fig. 5.

This new parameterization of the  $S$ -factor is closer to the calculations within the framework of Halo-EFT studied here and improves the description of the data, in particular for energies  $E_{\text{cm}} > 1$  MeV, and indeed yields a rate that is much smaller at higher temperatures, see Fig. 6.

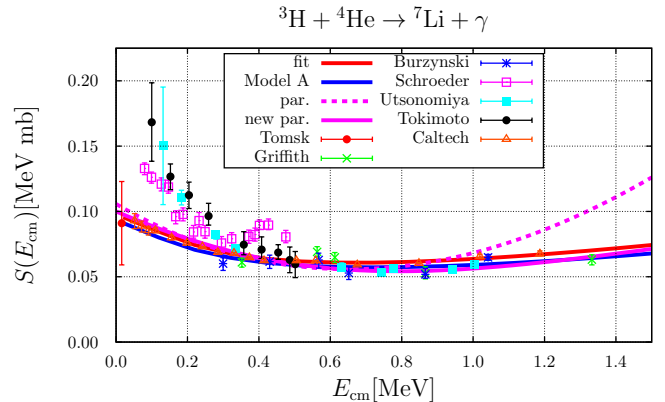


FIG. 5.  $S$ -factor as a function of the centre-of-mass energy compared to experimental data: Tomsk [46], Griffith [47], Burzynski [48], Schroeder [49], Utsonomiya [50–53], Tokimoto [54], Caltech [55]. The blue and red curve correspond to the parameter sets “A” and “fit”, respectively. The dotted purple curve represents the  $S$ -factor from the parameterization as used in Ref. [1]. The solid purple curve corresponds to the improved parameterization given in Eq. (45).

### D. The ${}^3\text{He} + {}^4\text{He} \rightarrow {}^7\text{Be} + \gamma$ reaction

In this case  $Z_v = 2$ ,  $Z_c = 2$ ,  $s_v = 1/2$ ,  $s_c = 0$  and  $Z_f = 4$  with  $J_f = 3/2$  for the ground state and  $J_f = 1/2$  for the first excited state. The radiative capture cross section is again determined by electric dipole contributions only, *i.e.* by the expression for the electric dipole contribution in Eqs. (10,12) with  $k_C \neq 0$ . The parameter sets labeled “fit” and “AII” correspond to the parameter sets labeled “ $\chi^2$ ” and “Model AII” in Ref. [8], respectively.

The astrophysical  $S$ -factor is displayed in Fig. 7. The resulting nominal rates are given in Fig. 8.

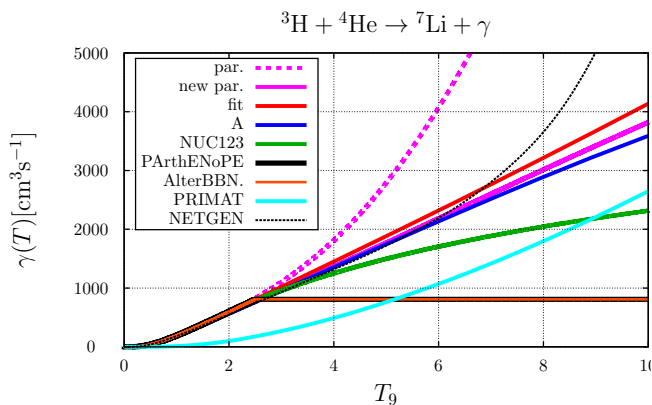


FIG. 6. Comparison of temperature ( $T_9 = T/10^9$  K) dependent rates for the  ${}^3\text{H} + {}^4\text{He} \rightarrow {}^7\text{Li} + \gamma$  reaction. The blue and red curve represents the parameter sets “A” and “fit”, respectively, the purple curve is the result corresponding to the parameterization of Eq. (45), while the dotted purple curve corresponds to the parameterization of Ref. [1]. Also shown are the parameterization of the rate as originally implemented in NUC123 [14] (green curve), PArthENoPE [17–19] (black curve), AlterBBN [15, 16] (brown curve) and PRIMAT [20] (cyan curve) as well as the parameterization provided by NETGEN, see [56].

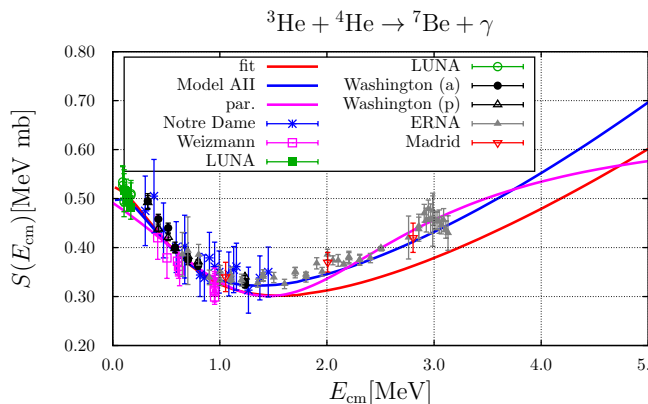


FIG. 7.  $S$ -factor as a function of the centre-of-mass energy compared to experimental data: Notre Dame [57], Weizmann [58], LUNA [59, 60], Washington [61], ERNA [62], Madrid [63]. The blue and red curve correspond to the parameter sets “A II” and “fit”, respectively. The purple curve represents the parameterization as used in Ref. [1].

#### IV. THE FINE-STRUCTURE CONSTANT DEPENDENCE OF THE RATES

In order to study the fine-structure constant dependence we calculated the rates for

$$\alpha = \alpha_0 (1 + \delta), \quad (46)$$

and the fractional change in  $\alpha$ , *i.e.*  $\delta$  was varied in the range  $[-0.05, +0.05]$ . We shall distinguish direct and indirect effects of the variation of the fine-structure constant:

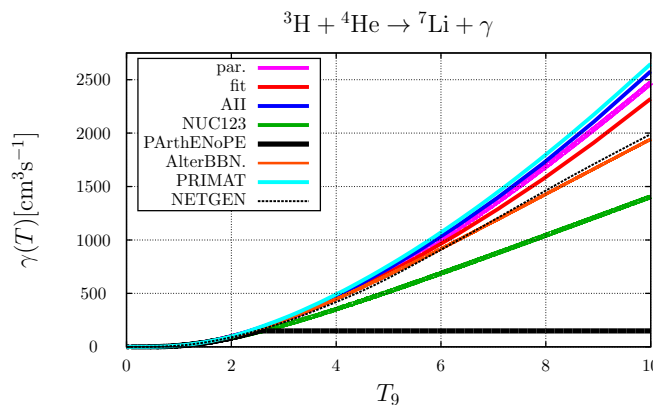


FIG. 8. Comparison of temperature ( $T_9 = T/10^9$  K) dependent rates for the  ${}^3\text{He} + {}^4\text{He} \rightarrow {}^7\text{Be} + \gamma$  reaction. The blue and red curve represent the parameter sets “AII” and “fit”, respectively, the purple curve corresponds to the parameterization of Ref. [1]. Also shown are the parameterizations of the rate as originally implemented in NUC123 [14] (green curve), PArthENoPE [17–19] (black curve), AlterBBN [15, 16] (brown curve) and PRIMAT [20] (cyan curve) as well as the parameterization provided by NETGEN, see [56].

*a. Direct effect* First of all the fine-structure constant  $\alpha$  enters the calculation of the radiative capture cross section as a linear factor due to the coupling of electromagnetic field to the charges and currents, which in the amplitude is proportional to  $e$  and hence in the cross section leads to a proportionality  $e^2 \propto \alpha$ . Furthermore  $\alpha$  enters the cross section via the inverse Bohr-radius  $k_C = Z_v Z_c c^2 \mu \alpha$ , that in turn determines the dimensionless quantities  $\eta_\gamma = k_C/\gamma$ , where  $\gamma$  is the binding momentum,  $\eta_\rho = k_C/\rho$ , where  $\rho$  the  $p$ -wave effective range, and  $\eta_p = k_C/p$  (the Sommerfeld-parameter), that enter the expressions for the normalization  $\mathcal{N}(\eta_\gamma, \eta_\rho)$  (Eq. (13)), the amplitudes  $\mathcal{A}(\eta_\gamma; \eta_\rho)$  (Eq. (16)), via  $X(\eta_\gamma; \eta_\rho)$  (Eq. (17)), and  $\mathcal{B}(\eta_\gamma; \eta_\rho)$  (Eq. (20)), as well as  $Y(\eta_\gamma; \eta_\rho)$  (Eq. (24)). The Sommerfeld-parameter  $\eta_p$  also enters the astrophysical  $S$ -factor.

Because the dependence of  $k_C$  on  $\alpha$  is linear,  $k_C \propto \alpha$ , we have

$$k_C(\alpha) = k_C(\alpha_0 (1 + \delta_\alpha)) = k_C(\alpha_0) (1 + \delta_\alpha). \quad (47)$$

We shall call this the “direct effect”.

*b. Indirect effect* On top of this, the value of  $\alpha$  influences the nuclear binding energies, *i.e.* the  $\alpha$  dependence of the nuclear mass of the nuclide  $i$  is given by

$$m^i(\alpha) = m_N^i + V_C^i (1 + \delta_\alpha) = m^i + V_C^i \delta_\alpha, \quad (48)$$

where  $V_C^i$  denotes the (repulsive) Coulomb-energy contribution to the nuclear mass. This in turn influences the  $Q$ -value of the reaction, *i.e.*

$$Q(\alpha) = m_v(\alpha) + m_c(\alpha) - M_f(\alpha) = B_f(\alpha) \quad (49)$$

and thus the binding momentum

$$\gamma(\alpha) = \sqrt{2\mu(\alpha)c^2 B_f(\alpha)}. \quad (50)$$

Concerning the kinematics of the reaction: For a given CMS kinetic energy  $E$ , the CMS relative momentum in the entrance channel  $p$  and the CMS final photon momentum  $k_\gamma$  are given by

$$s(E) = (m_v + m_c + E)^2, \quad (51)$$

$$p(E) = \sqrt{\frac{(s(E) - (m_c - m_v)^2)(s(E) - (m_c + m_v)^2)}{4s(E)}} \approx \sqrt{2\mu E}, \quad (52)$$

$$k_\gamma(E) = \frac{s(E) - M_f^2}{\sqrt{4s(E)}} \approx Q + E \quad (53)$$

and thus all depend on  $\alpha$ . Because in general (for  $\delta_\alpha \approx 0.1$ )  $\Delta V_C^i/m^i \approx \mathcal{O}(10^{-4})$  the dependence of  $M$  and  $\mu$  on  $\alpha$  is expected to be rather small ( $\Delta\mu/\mu \approx \mathcal{O}(10^{-4})$ ), whereas the change in the  $Q$ -value can be appreciable,  $\Delta Q/Q \approx \mathcal{O}(10^{-1})$ . Accordingly, the effect of a variation of  $\mu$  with a variation of  $\alpha$  on the value of  $k_C = Z_v Z_c \mu c^2 \alpha$  will be ignored.

We call the total of these kinematical variations the “indirect effect”.

In Ref. [1], we introduced an approximation to the dependence of the rate on  $\alpha$  by evaluating the effect on the parameterized  $S$ -factor at an energy where the  $S$ -factor is supposed to be maximal. For charged particle induced reactions this energy is given by

$$\bar{E} = \left(\frac{kT}{2}\right)^{\frac{2}{3}} (E_G^i)^{\frac{1}{3}}. \quad (54)$$

This then leads to a temperature dependent factor, that gives a fair approximation to parameterized results, both with and without including the indirect effects.

### A. The $n + {}^7\text{Li} \rightarrow {}^8\text{Li} + \gamma$ reaction

Since the neutron in the entrance channel is uncharged, there is no Coulomb interaction between the clusters and accordingly the direct effect of varying  $\alpha$ -dependence is completely determined by the fact that the cross section is strictly linear in  $\alpha$ . In addition there is the indirect effect stemming from the fine-structure constant dependence of the Coulomb contributions to the bindings energies of  ${}^7\text{Li}$  and  ${}^8\text{Li}$ , that affects the  $Q$ -value of the reaction.

The variation of the rate with  $\alpha$  is displayed in Fig. 9, where the relative variation  $\gamma(\alpha; T)/\gamma(\alpha_0; T)$  is plotted as a function of the temperature. Although the calculated rates, see Fig. 2, do differ slightly the relative changes of the rates are almost identical. The bottom panel in Fig. 9 indeed merely reflects that the cross section for this reaction trivially linearly depends on  $\alpha$ , *i.e.* if  $\alpha$  varies by 5%, then also the direct effect rate varies by 5% and this effect is temperature-independent. Small deviations occur if also the variation of the binding energies of the Li-nuclides is taken into account, see the top panel of Fig. 9.

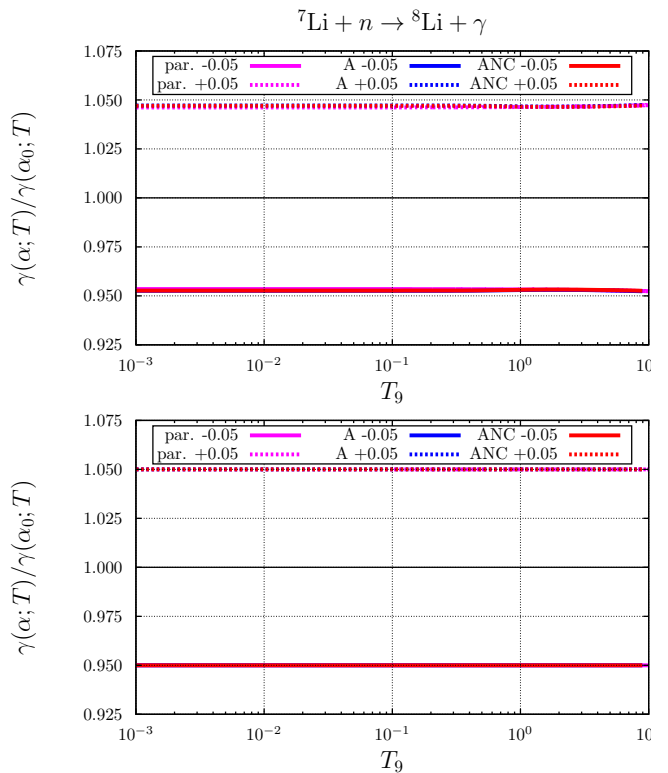


FIG. 9. Variation of the temperature ( $T_9 = T/10^9$  K) dependent rate for the  $n + {}^7\text{Li} \rightarrow {}^8\text{Li} + \gamma$  reaction with  $\alpha = \alpha_0(1 + \delta_\alpha)$ . The solid curves correspond to  $\delta = -0.05$ , the dotted lines to  $\delta = +0.05$ . Top panel: including both the direct and indirect effects; bottom panel: including the direct effect only.

### B. The $p + {}^7\text{Be} \rightarrow {}^8\text{B} + \gamma$ reaction

The fine-structure dependence of the temperature dependent rate of the proton-induced radiative capture reaction is more interesting. In Fig. 10 the variation of the temperature-dependent rate with  $\alpha$  of the calculated values with the two parameter sets is compared to the values obtained with the parameterization of the  $\alpha$ -dependence of the rates based on the parameterized cross sections as done in Ref. [1]. From this figure one infers that the relative variation in the Halo-EFT calculations is smaller by about 40% than that found in Ref. [1]. Excluding the  $M1$  contribution yields practically identical results. Furthermore it is observed, that considering also the indirect effect, *i.e.* also the effect on the binding energies and thus on the  $Q$ -value of the reaction, enhances this difference.

### C. The ${}^3\text{H} + {}^4\text{He} \rightarrow {}^7\text{Li} + \gamma$ reaction

The relative variation with  $\alpha$  of the temperature-dependent rate for the two parameter sets “fit” and “A” are compared to that with the rate based on the parame-

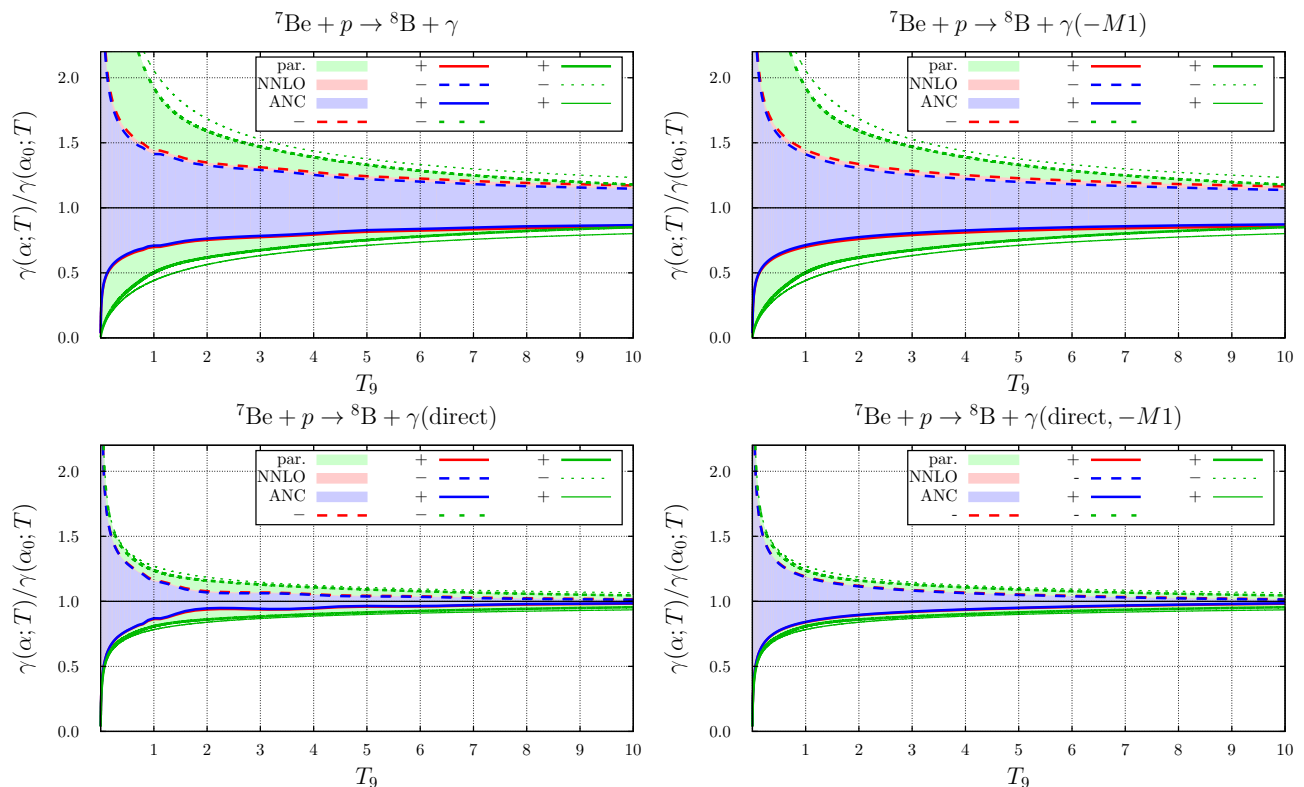


FIG. 10. Variation of the rate normalized to the rate at the nominal  $\alpha_0$  with varying  $\alpha$ , *i.e.*  $\gamma(T_9; \alpha_0(1 + \delta_\alpha))/\gamma(T_9; \alpha_0)$  for the  $p + {}^7\text{Be} \rightarrow {}^8\text{B} + \gamma$  reaction. Here,  $T_9 = T/10^9$  K. Top left: Total rate, including the  $M1$  contribution. Top right: Total rate, without the  $M1$  contribution. Bottom left: Direct variation only, including the  $M1$  contribution. Bottom right: Direct variation only, without the  $M1$  contribution. The coloured curves (areas) correspond to the variation of the rates with  $\alpha$  according to the penetration factor and the trivial linear dependence of the cross section on  $\alpha$  for dominant dipole radiation (direct effects). The blue and red curves (areas) represent the results for the parameter sets “ANC” and “NNLO”. The solid lines (marked ‘+’) correspond to  $\alpha = 0.05$ , the dotted lines to  $\alpha = -0.05$ . The thinner lines represent the results from the approximation to the fine-structure constant dependence of the rate based on the temperature-dependent factor evaluated at the energy  $E$  given in Eq. (54).

terization of Ref. [1] in Fig. 11. Contrary to the previous reaction this variation is larger for the Halo-EFT results, in particular for the parameter set “fit” than that with the parameterized rate. Considering the direct effect only leads to the same conclusion.

#### D. The ${}^3\text{He} + {}^4\text{He} \rightarrow {}^7\text{Be} + \gamma$ reaction

The relative variation of the rate with the value of the fine-structure constant  $\alpha$  of the temperature-dependent rates for the two parameter sets “fit” and “AII” are compared to that with the rate based on the parameterization of Ref. [1] in Fig. 12. Here, the relative variation with the two Halo-EFT parameter sets is much larger than for the parameterization used previously, in particular if the fine-structure constant is smaller than the nominal value. We shall discuss the reason for this in the next section, Sect. IV E.

#### E. Discussion

First of all we observe that although the resonant magnetic dipole contribution in the nucleon induced reaction accounts for a prominent feature in the cross sections (or astrophysical  $S$ -factors), this contribution is of minor importance in the variation of the rates with  $\alpha$ , see *e.g.* Fig. 10. Below we shall therefore focus on the effects from the dominant electric dipole contributions. With the exception of the neutron induced reaction the effects of the  $\alpha$ -variation differ from what was estimated on the basis of the parameterization of the cross-section used before in Ref. [1]. The dominant effect from the electric dipole contribution seems to be the  $\alpha$  variation of the normalisation of Eq. (13). The variation with  $\alpha$  of the relative normalisation  $N(\alpha)/N(\alpha_0)$  for the three charged particle induced reactions is displayed in Fig. 13. For the proton induced reaction the results are shown for both the  ${}^5P_2$  and the  ${}^3P_2$  amplitudes contributing with equal weight to the ground state capture. For the other two reactions the normalisation of the  ${}^2P_{3/2}$  (ground state) and the  ${}^2P_{1/2}$

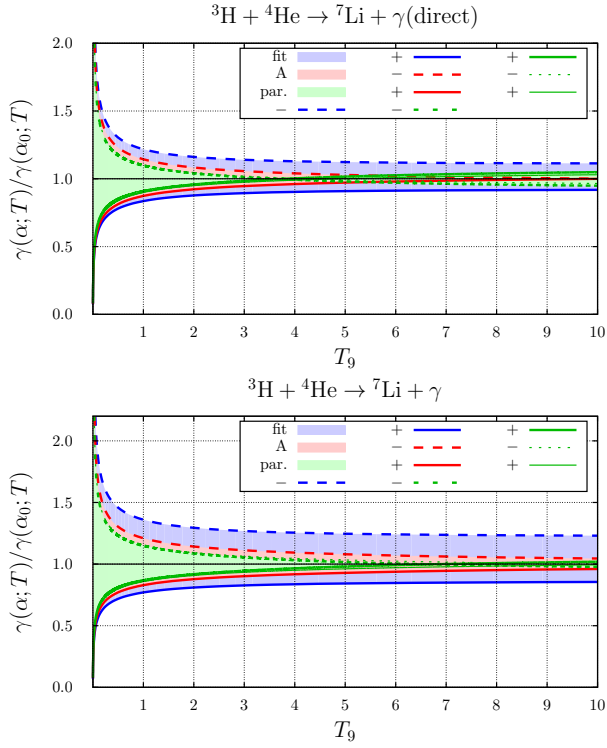


FIG. 11. Fine-structure constant dependence of the temperature dependent rate of the  ${}^3\text{H} + {}^4\text{He} \rightarrow {}^7\text{Li} + \gamma$  reaction. Shown is the rate relative to rate with the nominal value: “+” is the rate at  $\alpha = 1.05 \alpha_0$ , “-” the value at  $\alpha = 0.95 \alpha_0$ . Here,  $T_9 = T/10^9$  K. The blue ranges were obtained with the parameter set “fit”, the red range with the parameter set “A” and the green range represents the variation of  $\alpha$  as determined in Ref. [1]. The solid lines (marked ‘+’) correspond to  $\alpha = 0.05$ , the dotted lines to  $\alpha = -0.05$ . The fine-structure constant dependence of the rate based on the temperature dependent factor evaluated at the energy  $\bar{E}$  given in Eq. (54).

(excited state) are shown. This figure illustrates the main effects observed in the variation of the rates with  $\alpha$ :

1. Because of the absence of Coulomb interactions the variation with  $\alpha$  of the cross sections and corresponding rates of the neutron induced reaction is trivially linear.
2. For the proton induced reaction the normalisation varies with  $\alpha$  almost linearly by  $\pm 40\%$  for  $\delta \in [-0.05, 0.05]$ . Furthermore, the results for the two parameter sets considered here are almost identical. The variation of the rates is slightly larger for negative  $\delta$ , while considering the direct effect alone leads to a variation symmetric in  $\delta$ , in accordance with the variation of the normalisation. Also displayed in Fig. 10 is the variation of the parameterized rate with  $\alpha$  on the basis of the approximation introduced in Ref. [1], by evaluating the effects at a fixed energy, see also Eq. (54). Indeed for the proton induced reaction this temperature dependence is larger than the result calculated in Halo-EFT in

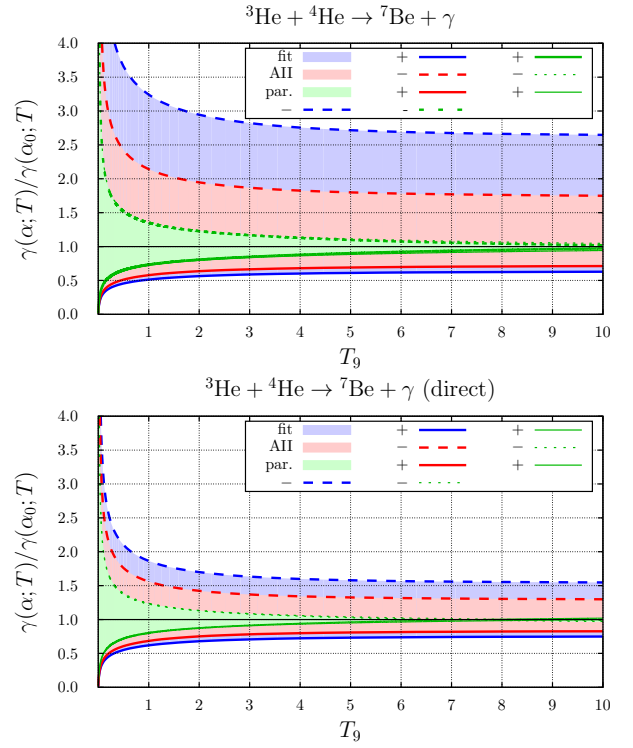


FIG. 12. Fine-structure constant dependence of the temperature dependent rate of the  ${}^3\text{He} + {}^4\text{He} \rightarrow {}^7\text{Be} + \gamma$  reaction. Here,  $T_9 = T/10^9$  K. Shown is the rate relative to rate with the nominal value: “+” is the rate at  $\alpha = 1.05 \alpha_0$ , “-” the value at  $\alpha = 0.95 \alpha_0$ . The blue ranges were obtained with the parameter set “fit”, the red range with the parameter set “A” and the green range represents the variation of  $\alpha$  as determined in Ref. [1]. The solid lines (marked ‘+’) correspond to  $\alpha = 0.05$ , the dotted lines to  $\alpha = -0.05$ . The fine-structure constant dependence of the rate based on the temperature dependent factor evaluated at the energy  $\bar{E}$  given in Eq. (54).

both cases.

3. In case of the  ${}^3\text{H}$  and  ${}^3\text{He}$  induced reactions the results with the approximation discussed above almost coincide with the results on the basis of the parameterization, as was already demonstrated in Ref. [1] and indeed in these cases is much smaller than what is to be expected on the basis of the normalisation. Anyhow, the  $\alpha$  dependence of the normalisation is rather asymmetric in  $\delta$  as shown in Fig. 13. For the  ${}^3\text{He}$  induced reaction this is even more prominent since the denominator in the expression for the norm, see Eq. (13), vanishes for  $\alpha < -0.06$ , corresponding to a pole in the normalisation and thus leading to a very asymmetric  $\delta$  dependence in this case.
4. Accordingly, within Halo-EFT the study of the  $\alpha$  dependence of the rates is limited to a rather moderate relative variation of  $\alpha$  of 5% only.

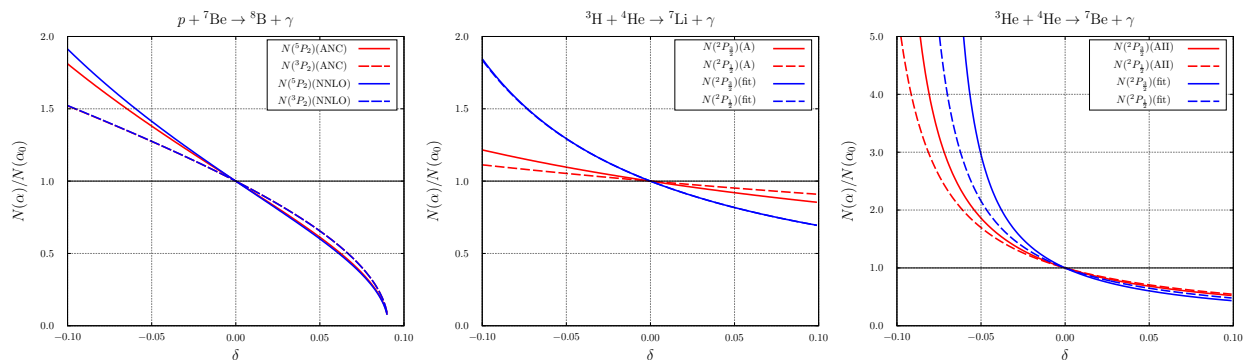


FIG. 13. Variation of the relative normalization  $N(\alpha)/N(\alpha_0)$  with  $\alpha = \alpha_0(1 + \delta)$  for the reactions  $p + {}^7\text{Be} \rightarrow {}^8\text{B} + \gamma$  (left),  ${}^3\text{H} + {}^4\text{He} \rightarrow {}^7\text{Li} + \gamma$  (middle),  ${}^3\text{He} + {}^4\text{He} \rightarrow {}^7\text{Be} + \gamma$  (right). For the first reaction the results are shown for both the  ${}^5P_2$  and the  ${}^3P_2$  amplitudes contributing with equal weight to the ground state capture. For the other two reactions the normalisation of the  ${}^2P_{3/2}$  (ground state) and the  ${}^2P_{1/2}$  (excited state) are shown. The first reaction ceases to be exo-energetic for positive  $\delta \approx 0.1$ . For the last reaction the expression for the normalisation, see Eq. (13), exhibits a pole for negative  $\delta \approx -0.06$ .

## V. ABUNDANCES

In order to assess the relevance of the variation of the rates with a variation of the fine-structure constant on the variation of the resulting abundances of the light elements in BBN, we used five different publicly available codes, *viz.* NUC123 [14], PArthENoPE [19], AlterBBN [16], PRIMAT [20] and PRyMordial [21, 22]. We use the rates as in our previous work, see [1], substituting the  $\alpha$  dependence of the rates for the four reactions considered here as discussed above. More specifically, for calculating the  $\alpha$  dependence of the abundances, we used the parameter sets “NNLO”, “fit” and “fit” for the  $p + {}^7\text{Be} \rightarrow {}^8\text{B} + \gamma$ ,  ${}^3\text{H} + {}^4\text{He} \rightarrow {}^7\text{Li} + \gamma$  and  ${}^3\text{He} + {}^4\text{He} \rightarrow {}^7\text{Be} + \gamma$  reactions, respectively, the  $\alpha$ -dependence of neutron induced radiative capture reaction  $n + {}^7\text{Li} \rightarrow {}^8\text{Li} + \gamma$  being practically linear anyway. As was demonstrated in the Sect. IV these parameter sets showed the largest variation of the rates with  $\alpha$ .

In Table IV we list the nominal rates, *i.e.* for  $\alpha = \alpha_0$ , see Eq. (40). The results show that with the exception of the values for the  ${}^7\text{Li}+\text{Be}$  abundance, which are larger by about 10%, and thus slightly deteriorate the so-called “Li-problem”, the treatment of the four reactions in Halo-EFT as considered here leads to results practically identical to those obtained previously in Ref. [1].

The fine-structure constant dependence of the primordial abundances is depicted in Fig. 14.

Again, the results for the  $d$ -,  ${}^3\text{H}+\text{He}$ -,  ${}^4\text{He}$ - and  ${}^6\text{Li}$ - abundances are very similar to those obtained previously, see Fig. 5 in Ref. [1]. Moreover, the five BBN-codes considered here produce consistent results, in spite of the fact that these codes differ in details, such as the number of reactions in the BBN network or the manner in which the rate equations are solved numerically. This then also applies to the values for the resulting response matrix elements. The (linear) response matrix elements  $\partial \log(Y_n/Y_H)/\partial \log \alpha = c_1$  and the coefficients

TABLE IV. Nominal abundances as number ratios  $Y_n/Y_H$  (for  ${}^4\text{He}$  the mass ratio  $Y_p$ ) calculated with the modified versions of the codes as in Ref. [1], but with the nominal results (*i.e.*  $\alpha = \alpha_0$ ) for the four reactions considered in this work. The value of the baryon-to-photon ratio and the nominal value of the neutron lifetime are  $\eta = 6.14 \cdot 10^{-10}$  and  $\tau_n = 879.4$  s, respectively. For comparison also the values previously obtained in Ref. [1] are listed.

code	${}^2\text{H}$ $\times 10^5$	${}^3\text{H}+\text{He}$ $\times 10^5$	$Y_p$	${}^6\text{Li}$ $\times 10^{14}$	${}^7\text{Li}+\text{Be}$ $\times 10^{10}$
NUC123	2.500	1.139	0.246	1.808	5.540
[1]	2.501	1.139	0.246	1.809	5.172
PArthENoPE	2.569	1.147	0.247	1.819	5.376
[1]	2.569	1.147	0.247	1.820	5.017
AlterBBN	2.585	1.153	0.248	1.903	5.350
[1]	2.585	1.153	0.248	1.904	4.993
PRIMAT	2.562	1.150	0.247	1.861	5.394
[1]	2.563	1.149	0.247	1.862	5.033
PRyMordial	2.581	1.148	0.247	1.891	5.448
PDG [13]	2.547		0.245		1.6
$\pm$	0.025		0.003		0.3

of the quadratic term ( $c_2$ ) in a quadratic least-squares fit of the form

$$P_k(\delta_\alpha) = c_0 (1 + c_1 \delta_\alpha + c_2 \delta_\alpha^2), \quad (55)$$

are given and compared to the results obtained previously in Table V.

We do find a very different result for the  $\alpha$ -dependence of the  ${}^7\text{Li}+\text{Be}$  abundance: In particular the linear response coefficient is approximately five times larger than the value obtained previously and moreover the response is far from linear, the quadratic coefficient being approximately 40 times larger than the value previously obtained in [1], as can also be seen from a comparison of Fig. 14 with Fig. 5 of Ref. [1].

If instead of the parameter sets “NNLO”, “fit” and “fit” for the reactions  $p + {}^7\text{Be} \rightarrow {}^8\text{B} + \gamma$ ,  ${}^3\text{H} + {}^4\text{He} \rightarrow$

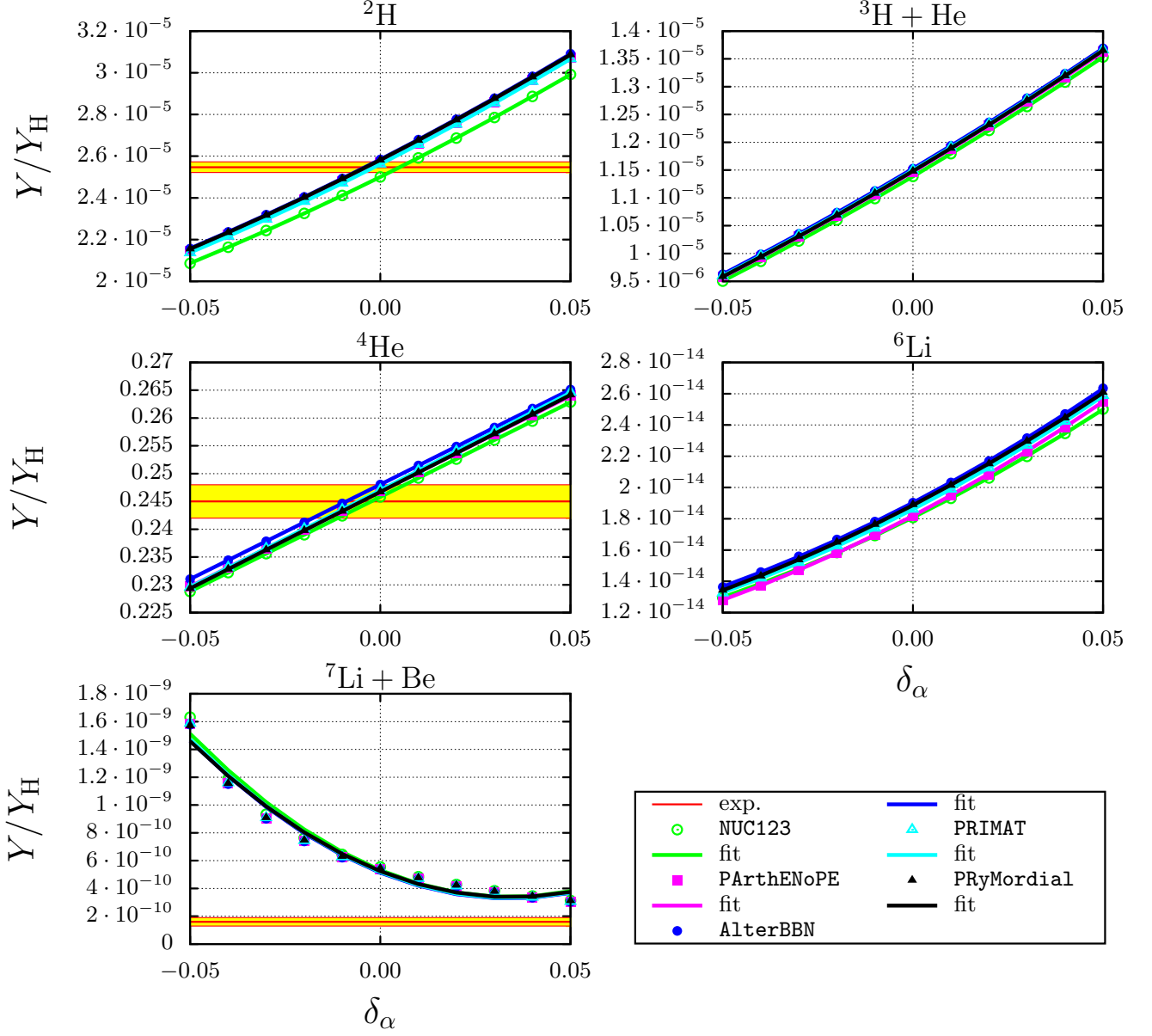


FIG. 14. Variation of the abundance ratios  $Y_n/Y_H$  with a variation of  $\alpha = \alpha_0(1 + \delta_\alpha)$  for  $\delta_\alpha \in [-0.05, 0.05]$  obtained with the codes: NUC123 [14], AlterBBN [16], PArthENoPE [19], PRIMAT [20] and PRyMordial [21, 22]. Here, we use  $\eta = 6.14 \cdot 10^{-10}$  and  $\tau_n = 879.4$  s. Also shown are the solid curves obtained by the fits according to Eq. (55) with the parameters listed in Table V. The experimental values cited in PDG [13] (thick red lines) are indicated by yellow-highlighted regions (color online) representing the  $1\sigma$  limits by red lines.

${}^7\text{Li} + \gamma$  and  ${}^3\text{He} + {}^4\text{He} \rightarrow {}^7\text{Be} + \gamma$ , respectively, we use the parameter sets “ANC”, “A” and “AII” of Tables II and III for these three reactions, respectively, we find similar results, except for the  ${}^7\text{Li} + \text{Be}$  response coefficients: In accordance with the fact that, as was shown in Sect. IV, the change of the rates with  $\alpha$  was found to be smaller for these parameters, the linear response coefficient  $c_1$  is about half as large and the quadratic coefficient is smaller by a factor 2.5, still corresponding to an appreciable curvature.

## VI. SUMMARY

In this work we have studied the fine-structure constant dependence of some BBN-relevant radiative capture reactions within the framework of Halo-EFT. We concentrated on the main effects, refraining from implementing a coupled channel approach as would be dictated by strict EFT power counting. Nevertheless we studied for each reaction two parameter sets in order to obtain an indication of the systematic errors. We found that the ef-

TABLE V. BBN response matrix  $c_1 = \partial \log(Y_n/Y_H)/\partial \log \alpha$  and the coefficients  $c_2$  of the quadratic term in Eq. (55) at  $\eta = 6.14 \cdot 10^{-10}$  and  $\tau_n = 879.4$  s.  $Y_n/Y_H$  are the number ratios of the abundances relative to hydrogen;  $Y_p$  is conventionally the  ${}^4\text{He}/\text{H}$  mass ratio. The results obtained with the five BBN codes NUC123 [14], PArthENoPE [19], AlterBBN [16], PRIMAT [20] and PRyMordial [21, 22] are compared to the results previously obtained in Ref. [1]. The odd rows show the results with the rates for the reactions evaluated in the present contribution for the reactions  $p + {}^7\text{Be} \rightarrow {}^8\text{B} + \gamma$ ,  ${}^3\text{H} + {}^4\text{He} \rightarrow {}^7\text{Li} + \gamma$  and  ${}^3\text{He} + {}^4\text{He} \rightarrow {}^7\text{Be} + \gamma$  where the parameter sets “NNLO”, “fit” and “fit” were used, respectively. Otherwise the rates are identical to those in [1].

code	${}^2\text{H}$		${}^3\text{H}+{}^3\text{He}$		$Y_p$		${}^6\text{Li}$		${}^7\text{Li}+{}^7\text{Be}$	
	$c_1$	$c_2$	$c_1$	$c_2$	$c_1$	$c_2$	$c_1$	$c_2$	$c_1$	$c_2$
NUC123	3.620	6.198	3.539	4.661	1.386	0.035	6.642	20.074	-21.296	312.074
[1]	3.655	6.228	3.540	4.625	1.387	0.016	6.830	20.412	-4.325	7.480
PArthENoPE	3.606	6.173	3.534	4.619	1.390	0.056	6.968	21.116	-21.284	312.328
[1]	3.635	6.182	3.533	4.577	1.389	0.065	7.159	21.482	-4.308	7.715
AlterBBN	3.610	6.135	3.526	4.591	1.375	0.048	6.651	20.167	-21.312	312.939
[1]	3.644	6.188	3.526	4.568	1.373	0.049	6.857	20.499	-4.322	7.865
PRIMAT	3.627	6.253	3.535	4.631	1.415	0.072	6.754	20.593	-21.273	311.595
[1]	3.658	6.264	3.534	4.595	1.408	0.081	6.953	20.828	-4.302	7.563
PRyMordial	3.609	5.975	3.544	4.756	1.411	0.081	6.698	18.453	-20.694	300.083

fects do deviate from what has been found previously on the basis of parameterized cross section data and a simple parameterization of the  $\alpha$  dependence motivated by a simple penetration factor. While for a neutron induced radiative capture reaction the results are almost strictly linear, as is to be expected since the radiative capture reaction amplitude is linear in the electromagnetic coupling and thus the cross section is linear in  $\alpha$ , for charged particle reactions the direct effect can both be smaller, as is the case for the  ${}^7\text{Be}(p, \gamma){}^8\text{B}$  reaction, or larger, as is the case for the  ${}^4\text{He}({}^3\text{H}, \gamma){}^7\text{Li}$  and the  ${}^4\text{He}({}^3\text{He}, \gamma){}^7\text{Be}$  radiative captures, than what is to be expected on the basis of the parameterized treatment.

In spite of these substantial deviations from the  $\alpha$ -dependence of the parameterized rates obtained for these reactions previously, the impact on the resulting abundances and on their  $\alpha$ -dependence of the light elements  ${}^2\text{H}$ ,  ${}^3\text{H}+{}^3\text{He}$ ,  ${}^4\text{He}$ ,  ${}^6\text{Li}$  with the rates calculated within the framework of Halo-EFT is very minor only. In contrast for the  ${}^7\text{Li}+{}^7\text{Be}$ -abundance we do find that the  $\alpha$ -dependence differs appreciably from that of the previous parameterized results, this  $\alpha$ -dependence being much more pronounced and clearly non-linear with the Halo-EFT rates. Also the nominal abundance (*i.e.* calculated with the current value of the fine-structure constant  $\alpha_0$ ) of  ${}^7\text{Li}+{}^7\text{Be}$  is larger by almost 10 %, whereas the other abundances remain practically unchanged.

For reactions involving charged particles, the Halo-EFT calculation accounts for the charged particle repulsion by inclusion of the full Coulomb propagator in all reaction steps. As the present study shows, these Coulomb effects cannot always be approximated by a universal penetration factor. It was also found that in some cases the study of the fine-structure dependence of cross sections and the corresponding rates within the framework of Halo-EFT can be limited by singularities appearing in the normalisation, that enters as a factor in the resulting cross sections. This was found to be rel-

evant for the  ${}^3\text{He} + {}^4\text{He} \rightarrow {}^7\text{Be} + \gamma$  reaction, limiting the study to relative variations of  $\alpha$  smaller than 6%. Furthermore, it should be stressed that the Halo-EFT framework is of course restricted to those reactions where the di-nuclear structure assumption underlying this is indeed applicable. Therefore a definite assessment of the fine-structure dependence of rates relevant for primordial nucleosynthesis should ultimately be performed within a framework that allows for a genuine *ab initio* treatment of nuclear reaction dynamics. Indeed recent progress within the framework of nuclear lattice effective field theory (NLEFT), see *e.g.* Ref. [64], shows that NLEFT seems to be a promising candidate for such a treatment.

## ACKNOWLEDGMENTS

We thank Daniel Phillips for a useful communication. This project is part of the ERC Advanced Grant “EXOTIC” supported the European Research Council (ERC) under the European Union’s Horizon 2020 research and innovation programme (grant agreement No. 101018170). We further acknowledge support by the Deutsche Forschungsgemeinschaft (DFG, German Research Foundation) and the NSFC through the funds provided to the Sino-German Collaborative Research Center TRR110 “Symmetries and the Emergence of Structure in QCD” (DFG Project ID 196253076 - TRR 110, NSFC Grant No. 12070131001), and the Chinese Academy of Sciences (CAS) President’s International Fellowship Initiative (PIFI) (Grant No. 2018DM0034).

### Appendix A: $C$ -integral

To calculate

$$\begin{aligned}
C(p) &= \lim_{\delta \downarrow 0} \frac{\mu^2}{6\pi^2(p^2 + \gamma^2)} \\
&\times \int_0^1 dx \int_0^1 dy \frac{1}{\sqrt{x(1-x)}} \frac{1}{\sqrt{1-y}} \\
&\left( x p^2 \log \left[ \frac{\pi}{4k_C^2} \left( -y p^2 + (1-y) \frac{\gamma^2}{x} - i\delta \right) \right] \right. \\
&+ p^2 \log \left[ \frac{\pi}{4k_C^2} \left( -y p^2 - (1-y) \frac{p^2}{x} - i\delta \right) \right] \\
&+ x \gamma^2 \log \left[ \frac{\pi}{4k_C^2} \left( y \gamma^2 + (1-y) \frac{\gamma^2}{x} - i\delta \right) \right] \\
&\left. + \gamma^2 \log \left[ \frac{\pi}{4k_C^2} \left( y \gamma^2 - (1-y) \frac{p^2}{x} - i\delta \right) \right] \right). \tag{A1}
\end{aligned}$$

Because the integral over  $y$  can be performed analytically this reduces to a single integral and, with the substitution  $x = \sin^2 \vartheta$ , one obtains with  $\kappa = \gamma/p$  and  $\eta_p = k_C/p$ :

$$\frac{C(p)}{\mu^2} = C_0 + C_1(\kappa), \tag{A2}$$

where

$$C_0 = \frac{1}{2\pi} \log \left[ \frac{\pi}{4\eta_p^2} \right] \tag{A3}$$

and

$$\begin{aligned}
C_1(\kappa) &= \frac{1}{3\pi^2(1 + \kappa^2)} \int_0^{\frac{\pi}{2}} d\vartheta \left\{ \sin^2 \vartheta c_1(\kappa; \sin^2 \vartheta) + c_2(\kappa; \sin^2 \vartheta) \right. \\
&\quad \left. + \sin^2 \vartheta \kappa^2 c_3(\kappa; \sin^2 \vartheta) + \kappa^2 c_4(\kappa; \sin^2 \vartheta) \right\},
\end{aligned}$$

to be evaluated numerically with the integrands

$$\begin{aligned}
c_1(\kappa; x) &= \int_0^1 dy \frac{1}{\sqrt{1-y}} \log \left[ -y + (1-y) \frac{\kappa^2}{x} - i\delta \right] \\
&= 2 \log \left[ \frac{\kappa^2}{x} \right] - 4 \\
&\quad + \frac{2}{\sqrt{\frac{\kappa^2}{x} + 1}} \left\{ \log \left[ \frac{\sqrt{\frac{\kappa^2}{x} + 1} + 1}{\sqrt{\frac{\kappa^2}{x} + 1} - 1} \right] - i\pi \right\} \tag{A4}
\end{aligned}$$

$$\begin{aligned}
c_2(\kappa; x) &= \int_0^1 dy \frac{1}{\sqrt{1-y}} \log \left[ -y - (1-y) \frac{1}{x} - i\delta \right] \\
&= -2 \log [x] - 2i\pi - 4 \\
&\quad + 4 \sqrt{\frac{x}{1-x}} \arctan \left( \sqrt{\frac{1-x}{x}} \right), \tag{A5}
\end{aligned}$$

$$\begin{aligned}
c_3(\kappa; x) &= \int_0^1 dy \frac{1}{\sqrt{1-y}} \log \left[ \kappa^2 y + (1-y) \frac{\kappa^2}{x} - i\delta \right] \\
&= 2 \log \left[ \frac{\kappa^2}{x} \right] - 4 \\
&\quad + 4 \sqrt{\frac{x}{1-x}} \arctan \left( \sqrt{\frac{1-x}{x}} \right), \tag{A6}
\end{aligned}$$

$$\begin{aligned}
c_4(\kappa; x) &= \int_0^1 dy \frac{1}{\sqrt{1-y}} \log \left[ \kappa^2 y - (1-y) \frac{1}{x} - i\delta \right] \\
&= -2 \log [x] - 2i\pi - 4 \\
&\quad + \frac{2\kappa}{\sqrt{\frac{1}{x} + \kappa^2}} \left\{ \log \left[ \frac{\sqrt{\frac{1}{x} + \kappa^2} + \kappa}{\sqrt{\frac{1}{x} + \kappa^2} - \kappa} \right] + i\pi \right\}. \tag{A7}
\end{aligned}$$

### Appendix B: $D'$ -integral

To calculate

$$\begin{aligned}
D'(k_C; p, \gamma) &= \lim_{\delta \downarrow 0} \frac{\mu^2}{6\pi^2(p^2 + \gamma^2)} \\
&\times \int_0^1 dx \int_0^1 dy \sqrt{\frac{x}{1-x}} \frac{1}{\sqrt{1-y}} \\
&\left( p^2 \log \left[ \frac{1}{4k_C^2} \left( -y p^2 + (1-y) \frac{\gamma^2}{x} - i\delta \right) \right] \right. \\
&+ p^2 \log \left[ \frac{1}{4k_C^2} \left( -y p^2 - (1-y) \frac{p^2}{x} - i\delta \right) \right] \\
&+ \gamma^2 \log \left[ \frac{1}{4k_C^2} \left( y \gamma^2 + (1-y) \frac{\gamma^2}{x} - i\delta \right) \right] \\
&\left. + \gamma^2 \log \left[ \frac{1}{4k_C^2} \left( y \gamma^2 - (1-y) \frac{p^2}{x} - i\delta \right) \right] \right). \tag{B1}
\end{aligned}$$

Thus, with  $\eta_p = k_C/p$  and  $\kappa = \gamma/p = \eta_p/\eta_\gamma$ :

$$\begin{aligned}
\frac{D'(\eta_p, \kappa)}{\mu^2} &= \lim_{\delta \downarrow 0} \frac{1}{6\pi^2(1 + \kappa^2)} \\
&\times \int_0^1 dx \int_0^1 dy \sqrt{\frac{x}{1-x}} \frac{1}{\sqrt{1-y}} \\
&\left( \log \left[ \frac{1}{4\eta_p^2} \left( -y + (1-y) \frac{\kappa^2}{x} - i\delta \right) \right] \right. \\
&+ \log \left[ \frac{1}{4\eta_p^2} \left( -y - (1-y) \frac{1}{x} - i\delta \right) \right] \\
&+ \kappa^2 \log \left[ \frac{1}{4\eta_p^2} \left( y \kappa^2 + (1-y) \frac{\kappa^2}{x} - i\delta \right) \right] \\
&\left. + \kappa^2 \log \left[ \frac{1}{4\eta_p^2} \left( y \kappa^2 - (1-y) \frac{1}{x} - i\delta \right) \right] \right),
\end{aligned}$$

*i.e.*

$$\begin{aligned} \frac{D'(\eta_p, \kappa)}{\mu^2} = & -\frac{1}{3\pi} \log(4\eta_p^2) \\ & + \frac{1}{3\pi^2(1+\kappa^2)} \int_0^{\frac{\pi}{2}} d\vartheta \sin^2\vartheta \\ & \left\{ c_1(\kappa, \sin^2\vartheta) + c_2(\kappa, \sin^2\vartheta) \right. \\ & \left. + \kappa^2 c_3(\kappa, \sin^2\vartheta) + \kappa^2 c_4(\kappa, \sin^2\vartheta) \right\}. \quad (\text{B2}) \end{aligned}$$

in terms of the integrands of Eqs. A4-A7 of Section A.

- 
- [1] U.-G. Meißner, B. C. Metsch and H. Meyer, Eur. Phys. J. A **59** (2023) no.10, 223 doi:10.1140/epja/s10050-023-01131-3 [arXiv:2305.15849 [hep-th]].
- [2] H. W. Hammer, C. Ji and D. R. Phillips, J. Phys. G **44** (2017) no.10, 103002 doi:10.1088/1361-6471/aa83db [arXiv:1702.08605 [nucl-th]].
- [3] G. Rupak, Nucl. Phys. A **678**, 405-423 (2000). doi:10.1016/S0375-9474(00)00323-7 [arXiv:nucl-th/9911018 [nucl-th]].
- [4] L. Fernando, R. Higa and G. Rupak, Eur. Phys. J. A **48** (2012), 24 doi:10.1140/epja/i2012-12024-7 [arXiv:1109.1876 [nucl-th]].
- [5] R. Higa, P. Premarathna and G. Rupak, Eur. Phys. J. A **57** (2021) no.9, 269 doi:10.1140/epja/s10050-021-00516-6 [arXiv:2009.09324 [nucl-th]].
- [6] R. Higa, P. Premarathna and G. Rupak, Phys. Rev. C **106** (2022) no.1, 014601 doi:10.1103/PhysRevC.106.014601
- [7] R. Higa, G. Rupak and A. Vaghani, Eur. Phys. J. A **54** (2018) no.5, 89 doi:10.1140/epja/i2018-12486-5 [arXiv:1612.08959 [nucl-th]].
- [8] P. Premarathna and G. Rupak, Eur. Phys. J. A **56** (2020) no.6, 166 doi:10.1140/epja/s10050-020-00113-z [arXiv:1906.04143 [nucl-th]].
- [9] X. Zhang, K. M. Nollett and D. R. Phillips, Phys. Rev. C **89** (2014) no.5, 051602 doi:10.1103/PhysRevC.89.051602 [arXiv:1401.4482 [nucl-th]].
- [10] X. Zhang, K. M. Nollett and D. R. Phillips, Phys. Lett. B **751** (2015), 535-540 doi:10.1016/j.physletb.2015.11.005 [arXiv:1507.07239 [nucl-th]].
- [11] X. Zhang, K. M. Nollett and D. R. Phillips, Phys. Rev. C **98** (2018) no.3, 034616 doi:10.1103/PhysRevC.98.034616 [arXiv:1708.04017 [nucl-th]].
- [12] X. Zhang, K. M. Nollett and D. R. Phillips, J. Phys. G **47** (2020) no.5, 054002 doi:10.1088/1361-6471/ab6a71 [arXiv:1909.07287 [nucl-th]].
- [13] R. L. Workman *et al.* [Particle Data Group], PTEP **2022**, 083C01 (2022). doi:10.1093/ptep/ptac097
- [14] L. Kawano, *Let's go: Early universe. 2. Primordial nucleosynthesis: The Computer way.* Report FERMILAB-PUB-92-004-A (1992).
- [15] A. Arbey, Comput. Phys. Commun. **183**, 1822-1831 (2012). doi:10.1016/j.cpc.2012.03.018 [arXiv:1106.1363 [astro-ph.CO]].
- [16] A. Arbey, J. Auffinger, K. P. Hickerson and E. S. Janssen, Comput. Phys. Commun. **248**, 106982 (2020). doi:10.1016/j.cpc.2019.106982 [arXiv:1806.11095 [astro-ph.CO]].
- [17] O. Pisanti, A. Cirillo, S. Esposito, F. Iocco, G. Mangano, G. Miele and P. D. Serpico, Comput. Phys. Commun. **178** 956-971 (2008). doi:10.1016/j.cpc.2008.02.015 [arXiv:0705.0290 [astro-ph]].
- [18] R. Consiglio, P. F. de Salas, G. Mangano, G. Miele, S. Pastor and O. Pisanti, Comput. Phys. Commun. **233**, 237-242 (2018). doi:10.1016/j.cpc.2018.06.022 [arXiv:1712.04378 [astro-ph.CO]].
- [19] S. Gariazzo, P. F. de Salas, O. Pisanti and R. Consiglio, Comput. Phys. Commun. **271**, 108205 (2022). doi:10.1016/j.cpc.2021.108205 [arXiv:2103.05027 [astro-ph.IM]].
- [20] C. Pitrou, A. Coc, J. P. Uzan and E. Vangioni, Phys. Rept. **754**, 1-66 (2018). doi:10.1016/j.physrep.2018.04.005 [arXiv:1801.08023 [astro-ph.CO]].
- [21] A.-K. Burns, T. M. P. Tait and M. Valli, [arXiv:2307.07061 [hep-ph]] (2023).
- [22] A.-K. Burns, T. M. P. Tait and M. Valli, <https://github.com/vallima/PRyMordial>
- [23] Y. Nagai, M. Igashira, T. Takaoka, T. Kikuchi, T. Shima, A. Tomyo, A. Mengoni and T. Otsuka, Phys. Rev. C **71** (2005), 055803 doi:10.1103/PhysRevC.71.055803
- [24] W. L. Imhof, R. G. Johnson, F. J. Vaughn and M. Walt, Phys. Rev. **114** (1959), 1037-1039 doi:10.1103/PhysRev.114.1037 PIRE as of 06 Feb 2024
- [25] J. Gorres, M. Wiescher, S. Graff, R. B. Vogelaar, B. W. Filippone, C. A. Barnes, S. E. Kellogg, T. R. Wang and B. A. Brown, Phys. Rev. C **39** (1989), 8-13 doi:10.1103/PhysRevC.39.8
- [26] R. B. Firestone and Z. Revay, Phys. Rev. C **93** (2016) no.5, 054306 doi:10.1103/PhysRevC.93.054306
- [27] E. A. Koltypin and V. M. Morozov, Dokl. 1 (1956) 65
- [28] J. E. Lynn, E. T. Journey and S. Raman, Phys. Rev. C **44** (1991), 764-773 doi:10.1103/PhysRevC.44.764
- [29] M. Heil, F. K appler, M. Wiescher, A. Mengoni, Astrophys. J. 507, 1002 (1998)
- [30] J. C. Blackmon, A. E. Champagne, J. K. Dickens, J. A. Harvey, M. A. Hofstee, S. Kopecky, D. C. Larson, D. C. Powell, S. Raman and M. S. Smith, Phys. Rev. C **54** (1996), 383-388 doi:10.1103/PhysRevC.54.383
- [31] R. Buompane, A. Di Leva, L. Gialanella, A. D'Onofrio, M. De Cesare, J. G. Duarte, Z. F ul op, L. R. Gasques, G. Gy urky and L. Morales-Gallegos, *et al.* Phys. Lett. B

- 824** (2022), 136819 doi:10.1016/j.physletb.2021.136819
- [32] A. R. Junghans, K. A. Snover, E. C. Mohrmann, E. G. Adelberger and L. Buchmann, *Phys. Rev. C* **81** (2010), 012801 doi:10.1103/PhysRevC.81.012801
- [33] A. R. Junghans, E. C. Mohrmann, K. A. Snover, T. D. Steiger, E. G. Adelberger, J. M. Casandjian, H. E. Swanson, L. Buchmann, S. H. Park and A. Zyuzin, *et al.* *Phys. Rev. C* **68** (2003), 065803 doi:10.1103/PhysRevC.68.065803 [arXiv:nucl-ex/0308003 [nucl-ex]].
- [34] A. R. Junghans, E. C. Mohrmann, K. A. Snover, T. D. Steiger, E. G. Adelberger, J. M. Casandjian, H. E. Swanson, L. Buchmann, S. H. Park and A. Zyuzin, *Phys. Rev. Lett.* **88** (2002), 041101 doi:10.1103/PhysRevLett.88.041101 [arXiv:nucl-ex/0111014 [nucl-ex]].
- [35] A. R. Junghans, E. C. Mohrmann, K. A. Snover, T. D. Steiger, E. G. Adelberger, J. M. Casandjian, H. E. Swanson, L. R. Buchmann, A. M. Laird and S. Park, *et al.* *Nucl. Phys. A* **746** (2004), 210-214 doi:10.1016/j.nuclphysa.2004.09.035
- [36] L. T. Baby *et al.* [ISOLDE], *Phys. Rev. C* **67** (2003), 065805 [erratum: *Phys. Rev. C* **69** (2004), 019902] doi:10.1103/PhysRevC.69.019902 [arXiv:nucl-ex/0212011 [nucl-ex]].
- [37] L. T. Baby *et al.* [ISOLDE], *Phys. Rev. Lett.* **90** (2003), 022501 [erratum: *Phys. Rev. Lett.* **92** (2004), 029901] doi:10.1103/PhysRevLett.90.022501 [arXiv:nucl-ex/0208005 [nucl-ex]].
- [38] L. T. Baby *et al.* [ISOLDE], *Nucl. Phys. A* **718** (2003), 487-489 doi:10.1016/S0375-9474(03)00865-0
- [39] F. Strieder, L. Gialanella, G. Gyürky, F. Schümann, R. Bonetti, C. Broggin, L. Campajola, P. Corvisiero, H. Costantini and A. D'Onofrio, *et al.* *Nucl. Phys. A* **696** (2001), 219-230 doi:10.1016/S0375-9474(01)01121-6
- [40] F. Hammache, G. Bogaert, P. Aguer, C. Angulo, S. Barhoumi, L. Brillard, J. F. Chemin, G. Claverie, A. Coc and M. Hussonnois, *et al.* *Phys. Rev. Lett.* **80** (1998), 928-931 doi:10.1103/PhysRevLett.80.928 [arXiv:nucl-ex/9712003 [nucl-ex]].
- [41] B. W. Filippone and A. J. Elwyn, C. N. Davids and D. D. Koetke, *Phys. Rev. C* **28** (1983), 2222-2229 doi:10.1103/PhysRevC.28.2222
- [42] B. W. Filippone, A. J. Elwyn, C. N. Davids and D. D. Koetke, *Phys. Rev. Lett.* **50** (1983), 412-416 doi:10.1103/PhysRevLett.50.412
- [43] F. J. Vaughn, R. A. Chalmers, D. Kohler and L. F. Chase, *Phys. Rev. C* **2** (1970), 1657-1665 doi:10.1103/PhysRevC.2.1657
- [44] R. W. Kavanagh, *Nucl. Phys.* **15** (1960), 411-420 [https://doi.org/10.1016/0029-5582\(60\)90322-9](https://doi.org/10.1016/0029-5582(60)90322-9).
- [45] P. D. Parker, *Phys. Rev.* **150** (1966), 851-856 doi:10.1103/PhysRev.150.851
- [46] V. M. Bystritsky, G. N. Dudkin, E. G. Emets, M. Filipowicz, A. R. Krylov, B. A. Nechaev, A. Nurkin, V. N. Padalko, A. V. Philippov and A. B. Sadvovskiy, *Phys. Part. Nucl. Lett.* **14** (2017) no.4, 560-570 doi:10.1134/S1547477117040057
- [47] G. M. Griffith, R. A. Morrow, P. J. Riley, J. B. Warren, *Can. J. Phys.* **39** (1961), 1397
- [48] S. Burzyński, K. Czerski, A. Marcinkowski and P. Zupranski, *Nucl. Phys. A* **473** (1987), 179-188 doi:10.1016/0375-9474(87)90160-6
- [49] U. Schröder, A. Redder, C. Rolfs, R. E. Azuma, L. Buchmann, C. Campbell, J. D. King and T. R. Donoghue, *Phys. Lett. B* **192** (1987), 55-58 doi:10.1016/0370-2693(87)91141-5
- [50] H. Utsunomiya, R. P. Schmitt, Y. W. Lui, D. R. Haenni, H. Dejbakhsh, L. Cooke, P. Heimberg, A. Ray, T. Tamura and T. Udagawa, *Phys. Lett. B* **211** (1988), 24-28 doi:10.1016/0370-2693(88)90800-3
- [51] H. Utsunomiya, Y. W. Lui, L. Cooke, H. Dejbakhsh, D. R. Haenni, P. Heimberg, A. Ray, B. K. Srivastava, R. P. Schmitt and T. Udagawa, *Nucl. Phys. A* **511** (1990), 379-406 doi:10.1016/0375-9474(90)90165-I
- [52] H. Utsunomiya, Y. W. Lui, D. R. Haenni, H. Dejbakhsh, L. Cooke, B. K. Srivastava, W. Turmel, D. O'Kelly, R. P. Schmitt and D. Shapira, *et al.* *Phys. Rev. Lett.* **65** (1990), 847-850 doi:10.1103/PhysRevLett.65.847
- [53] H. Utsunomiya, Y.-W. Lui, S. R. Haenni, H. Dejbakhsh, L. Cooke, B. K. Srivastava, W. Turmel, D. O'Kelly, R. P. Schmitt, D. Shapira, J. Gomez del Campo, A. Ray, T. Udagawa, *Phys. Rev. Lett.* **69** (1992), 863-863(E) doi:10.1103/PhysRevLett.69.863.2
- [54] Y. Tokimoto, H. Utsunomiya, T. Yamagata, M. Ohta, Y. W. Lui, R. P. Schmitt, S. Typel, Y. Aoki, K. Ieki and K. Katori, *Phys. Rev. C* **63** (2001), 035801 doi:10.1103/PhysRevC.63.035801
- [55] C. R. Brune, R. W. Kavanagh and C. Rolfs, *Phys. Rev. C* **50** (1994), 2205-2218 doi:10.1103/PhysRevC.50.2205
- [56] Y. Xu, S. Goriely, A. Jorissen, G. Chen and M. Arnould, *Astron. Astrophys.* **549**, A106 (2013).
- [57] A. Kontos, E. Uberseder, R. deBoer, J. Görres, C. Akers, A. Best, M. Couder and M. Wiescher, *Phys. Rev. C* **87** (2013) no.6, 065804 doi:10.1103/PhysRevC.87.065804
- [58] B. S. Nara Singh, M. Hass, Y. Nir-El and G. Haquin, *Phys. Rev. Lett.* **93** (2004), 262503 doi:10.1103/PhysRevLett.93.262503 [arXiv:nucl-ex/0407017 [nucl-ex]].
- [59] G. Gyurky, F. Confortola, H. Costantini, A. Formicola, D. Bemmerer, R. Bonetti, C. Broggin, P. Corvisiero, Z. Elekes and Z. Fulop, *et al.* *Phys. Rev. C* **75** (2007), 035805 doi:10.1103/PhysRevC.75.035805 [arXiv:nucl-ex/0702003 [nucl-ex]].
- [60] F. Confortola *et al.* [LUNA], *Phys. Rev. C* **75** (2007), 065803 doi:10.1103/PhysRevC.75.065803 [arXiv:0705.2151 [nucl-ex]].
- [61] T. A. D. Brown, C. Bordeanu, K. A. Snover, D. W. Storm, D. Melconian, A. L. Sallaska, S. K. L. Sjue and S. Triambak, *Phys. Rev. C* **76** (2007), 055801 doi:10.1103/PhysRevC.76.055801 [arXiv:0710.1279 [nucl-ex]].
- [62] A. Di Leva, L. Gialanella, R. Kunz, D. Rogalla, D. Schurmann, F. Strieder, M. De Cesare, N. De Cesare, A. D'Onofrio and Z. Fulop, *et al.* *Phys. Rev. Lett.* **102** (2009), 232502 [erratum: *Phys. Rev. Lett.* **103** (2009), 159903] doi:10.1103/PhysRevLett.102.232502
- [63] M. Carmona-Gallardo, B. S. Nara Singh, M. J. G. Borge, J. A. Briz, M. Cubero, B. R. Fulton, H. Fynbo, N. Gordillo, M. Hass and G. Haquin, *et al.* *Phys. Rev. C* **86** (2012), 032801 doi:10.1103/PhysRevC.86.032801
- [64] S. Elhatisari, T. A. Lähde, D. Lee, U.-G. Meißner and T. Vonk, *JHEP* **02**, 001 (2022). doi:10.1007/JHEP02(2022)001 [arXiv:2112.09409 [hep-th]].